Physics of microscopic vehicular traffic prediction for automated driving

Boris S. Kerner[1] and Sergey L. Klenov[2]
[1]*Physics of Transport and Traffic, University of Duisburg-Essen, 47048 Duisburg, Germany*
[2]*Moscow Institute of Physics and Technology, Department of Physics, 141700 Dolgoprudny, Moscow Region, Russia*

(Received 25 July 2022; accepted 9 September 2022; published 28 October 2022)

With the use of microscopic traffic simulations, physical features of *microscopic traffic prediction* for automated driving that should improve traffic harmonization and safety have been found: During a short-time prediction horizon (about 10 s), online prediction of the locations and speeds of all vehicles in some limited area around the automated-driving vehicle is possible; this enables the automated vehicle control in complex traffic situations in which the automated-driving vehicle is not able to make a decision based on current traffic information without the use of the microscopic traffic prediction. Through a more detailed analysis of an unsignalized city intersection, when the automated vehicle wants to turn right from a secondary road onto the priority road, the statistical physics of the effect of a data uncertainty caused by errors in data measurements on the prediction reliability has been studied: (i) probability of the prediction reliability has been found; (ii) there is a critical uncertainty, i.e., a maximum amplitude of errors in data measurements: when the uncertainty does not exceed the critical uncertainty, the prediction reliability probability is equal to 1, otherwise, the prediction is not applicable for a reliable automated vehicle control; (iii) physical characteristics of the microscopic traffic prediction, at which the critical uncertainty can be increased considerably, have been found; and (iv) there is an optimal automated vehicle control at which the critical uncertainty reaches a maximum value.

DOI: 10.1103/PhysRevE.106.044307

I. INTRODUCTION

Since the 1950s–1960s, many microscopic traffic flow models in which the motion of each vehicle in traffic flow can be simulated were introduced (e.g., classical car-following models by Reuschel [1–3], Pipes [4], Kometani and Sasaki [5–8], Chandler, Herman, Gazis, Rothery, Montroll, and Potts [9–12], and Newell [13]. During the last 70 years, a huge number of other car-following models were developed (see, e.g., Refs. [14–25]). In the car-following models, the microscopic characteristics of the motion of the preceding vehicle related to a time instant have been used to determine the acceleration of the following vehicle that should be chosen at the time instant. In some of the models, additionally, microscopic characteristics of other vehicles in a vicinity of the vehicle have been taken into account.

Recently, two other fields of the physics of vehicular traffic have been developed: (i) *automated-driving vehicles in mixed traffic flow* consisting of a random distribution of human-driving and automated-driving vehicles [automated vehicle (AV)] [26–33] and (ii) *vehicular networking*, i.e., a vehicular network in which vehicles can communicate with each other through vehicle-to-vehicle communication and/or through vehicle-to-infrastructure communication; both types of vehicular communications are called V2X communication (see, e.g., Refs. [34–40]). Through V2X communication, an automated vehicle can have additional information about the behaviors of other vehicles in the neighborhood of the automated vehicle. This information can be used for short-time prediction of a traffic situation, for example, based on a so-called partially observable Markov decision process [41–45] and learning algorithms [46–48], as well as many other artificial intelligence and model approaches (see, e.g., Refs. [49–58]). The short-time prediction of traffic situations in the neighborhood of the automated vehicle is required for the planning of the trajectory of the automated vehicle.

In this paper, we study the physics of a qualitative different approach for the short-time traffic prediction for automated driving based on microscopic traffic simulations [59]. In this *physical approach* based on the microscopic physics of vehicular traffic, the microscopic traffic prediction is made through simulations of car-following models for mixed traffic flow [59].

Contrary to the well-known approach for microscopic traffic simulations of *the actual traffic situation* [1–25], in this paper we apply microscopic traffic simulations for the *microscopic traffic prediction* made during a short-time prediction horizon (about 10 s).

The term *microscopic traffic prediction* used in this paper means that in some limited area around the automated vehicle, the microscopic traffic prediction of the locations and speeds of all vehicles is performed during the short-time prediction horizon. The microscopic traffic flow model for mixed traffic can include different mathematical rules of vehicle motion for different types of human-driving and automated-driving vehicles. The methodology of microscopic prediction for automated driving can also be considered an application of vehicular networking. This is because vehicular networking is needed for both the data reconstruction of a microscopic traffic situation around the automated vehicle and for providing the data to the vehicle.

The paper is organized as follows. In Sec. II, we present the methodology of physical modeling of the microscopic

prediction in vehicular traffic, discuss an application scenario of the microscopic traffic prediction studied in the paper, and consider a microscopic model of mixed traffic flow used for simulations. The physics of the microscopic traffic prediction is presented in Sec. III. The effect of the uncertainty of the data of microscopic traffic situations on the microscopic traffic prediction is considered in Sec. IV. Stochastic physical features of the microscopic traffic prediction under data uncertainty are revealed in Sec. V. A critical uncertainty in the data is studied in Sec. VI. In Sec. VII, we show that there is some optimal automated vehicle control at which the critical uncertainty reaches its maximum value. In Sec. VIII, we present a qualitative discussion of some other possible applications of the microscopic traffic prediction (Sec. VIII A) as well as formulating conclusions (Sec. VIII B).

II. METHODOLOGY OF PHYSICAL MODELING OF MICROSCOPIC PREDICTION IN VEHICULAR TRAFFIC

A. General description

We assume that through vehicular networking at some time instants

$$t = t_p, \ \ p = 1, 2, 3, \ldots, \tag{1}$$

locations (including the correspondence to road lanes) and speeds of all vehicles moving around an automated vehicle are known. We call the multitude of the vehicle locations x and vehicle speeds v as *a microscopic traffic situation* at time instant t_p. A time interval $\delta t = t_{p+1} - t_p$ that can be very small (e.g., between 0.1 s and 1 s) should not necessarily be a constant value; this time interval is determined by the measurement technology of the microscopic traffic situation. The methodology for the short-time microscopic traffic prediction is as follows:

(i) A microscopic traffic situation at time instant t_p is used as an initial condition for a microscopic traffic flow model of mixed vehicular traffic.

(ii) For any time instant t_p, the microscopic traffic flow model calculates future (predicted) microscopic traffic situations that the model predicts for a prediction horizon ΔT_p. Thus, for each of the given time instants t_p, the microscopic model calculates the vehicle locations and vehicle speeds during prediction horizon ΔT_p. This microscopic traffic prediction is only possible when the microscopic model is able to calculate the traffic prediction during a negligible short time interval in comparison with time interval $\delta t = t_{p+1} - t_p$.

It should be emphasized that the time-discrete traffic flow model for mixed traffic used in the paper (see Sec. II C) is able to calculate a microscopic traffic prediction during a negligible short time interval $\theta < 0.005$ s [60].

(iii) The prediction of the vehicle locations and vehicle speeds are used for the calculation of the future trajectory of the automated vehicle.

(iv) All stages (i)–(iii) explained above are repeated at the next time instant t_{p+1}, when a different microscopic traffic situation is known. This microscopic traffic situation is used as an initial condition for the microscopic traffic flow model. Then, the model makes the microscopic traffic prediction for vehicle locations and vehicle speeds during prediction horizon ΔT_{p+1} (prediction horizon ΔT_p can be different for different time instants t_p). Then, stages (i)–(iii) are iterated for each new time instant t_{p+2}, t_{p+3}, and so on, once data for new microscopic traffic situations are available for the automated vehicle through the use of vehicular networking. Thus, in the approach there is repetition of the microscopic traffic prediction for any current time instant t_p (1) at which microscopic traffic situations are available. This allows us to update the calculation of the trajectory of the automated vehicle during the vehicle motion in mixed traffic flow.

B. Application of microscopic traffic prediction for unsignalized intersection in city traffic

In a general case, the prediction of the motion of the local neighbors for the automated vehicle can depend on the behavior of the automated vehicle, whereas the behavior of the automated vehicle depends on the motion of the neighbor vehicles. This means that the methodology for microscopic traffic prediction discussed in Sec. II A can only be used in traffic situations in which either the predicted motion of the local neighboring vehicles does not depend on the automated vehicle motion or the dependence of the predicted motion of the local neighbors on the automated vehicle motion is not important for the automated vehicle control realized through the use of the microscopic traffic prediction.

As explained in Sec. VIII A, there are a number of such traffic situations. For each of the traffic situations, mathematical conditions for the motion of the automated vehicle following from the microscopic traffic prediction can be very different. For this reason, we limit a study of physical features of the microscopic traffic prediction through the analysis of a very often case in city traffic in which the automated vehicle (black vehicle in Fig. 1) moves initially on a secondary road and it would like to turn right onto a priority road. There is no traffic signal on the city intersection of these two roads. The objective of the microscopic traffic prediction is to find whether there is a possibility for merging the automated vehicle onto the priority road *without stopping* at the intersection. If such a possibility exits, then the automated vehicle motion is controlled through the use of the microscopic traffic prediction.

In this application (Fig. 1), the predicted motion of the local neighboring vehicles calculated through microscopic prediction does not depend on the automated vehicle motion. A microscopic traffic situation measured at time instant $t = t_{\rm p}$ is qualitatively shown in Fig. 1(a). Only the local neighboring vehicles that future motion can be relevant for the automated vehicle control are used (these red colored vehicles are within a red colored dashed region). In Fig. 1(b), speeds and locations of these vehicles are put into the same region in the model of the microscopic traffic prediction (old vehicles that were at $t < t_{\rm p}$ in the region are removed). Then, the calculation of the microscopic traffic prediction is performed.

Through this prediction, deceleration b_p of the automated vehicle during time interval $t_p \leqslant t \leqslant t_{\rm E}$ is found, where $t_{\rm E}$ is a *predicted* time instant at which the vehicle should turn right onto the priority road ($t_{\rm E} \leqslant t_{\rm p} + \Delta T_{\rm p}$) [Fig. 1(c)]. However, in accordance with Sec. II A, the automated vehicle decelerates

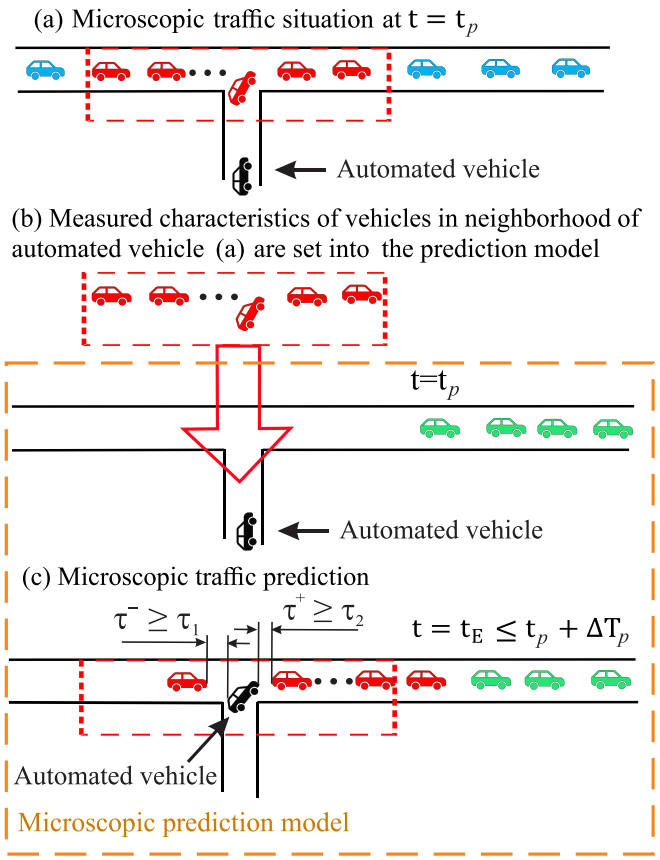

FIG. 1. Qualitative explanation of microscopic traffic prediction for an unsignalized intersection in city traffic. (a) Microscopic traffic situation measured at $t = t_p$ (1); only red-colored vehicles that are in a red-colored dashed road region can affect on the motion of the automated vehicle (black-colored vehicle). (b) The measured characteristics of red-colored vehicles (vehicle speeds, vehicle locations, vehicle lengths, and so on) in the red-colored dashed road region shown in (a) are used in the microscopic prediction model; before, all vehicles that were at $t < t_p$ in this dashed road region of the microscopic prediction model are removed. (c) Through the use of the microscopic traffic prediction, a predicted time instant t_E is found at which the vehicle should turn right onto the priority road.

with the deceleration b_p only during a time interval

$$t_p \leqslant t < t_{p+1}, \tag{2}$$

where $t = t_{p+1}$ is the time instant at which the next microscopic traffic situation is known. At $t = t_{p+1}$, the same procedure of microscopic traffic prediction shown in Fig. 1 is repeated for $t = t_{p+1}$ leading to a new deceleration b_{p+1} and a new predicted time instant t_E at which the vehicle should turn right onto the priority road; the new deceleration b_{p+1} is applied only during the time interval $t_{p+1} \leqslant t < t_{p+2}$, and so on. Because microscopic traffic situations depend on time t_p (1), all predicted values (like the above-mentioned predicted time instant t_E) are functions of the time instant t_p at which the prediction is made.

It should be emphasized that in the microscopic traffic prediction made at each $t = t_p$ (1), some safety conditions for the automated vehicle merging at the predicted time instant t_E should be satisfied,

$$\tau^- \geqslant \tau_1, \ \tau^+ \geqslant \tau_2, \tag{3}$$

where τ^- is the time headway of a vehicle following the automated vehicle on the priority road just after merging, τ^+ is time headway of the automated vehicle to the preceding vehicle on the priority road just after merging, and τ_1 and τ_2 are model parameters. After the automated vehicle has merged onto the priority road, we have assumed that no microscopic traffic prediction is needed.

C. Microscopic model of mixed traffic flow

There are a huge number of different microscopic traffic flow models for mixed traffic (see, e.g., Refs. [61–73]). A basic requirement of a model for simulations of the microscopic traffic prediction is that the model should simulate microscopic behavior of human drivers in different traffic situations as close as possible to real measured traffic data. We use the model for mixed traffic of Ref. [73] because, as explained in Refs. [74,75], the model satisfies this basic requirement. There are different rules of motion for human- and automated-driving vehicles in the model. Updated rules of motion of human-driving vehicles in a road lane are [74,76–78]

$$v_{n+1} = \max(0, \min(v_{\text{free}}, \widetilde{v}_{n+1} + \xi_n, v_n + a_{\max}\tau, v_{s,n})), \tag{4}$$

$$x_{n+1} = x_n + v_{n+1}\tau. \tag{5}$$

The index n corresponds to discrete time $n\tau$, $n = 0, 1, \ldots$, $\tau = 1$ s; x_n and v_n are, respectively, the vehicle location and speed at time step n; $a_{\max}$ is a maximum acceleration; $g_n = x_{\ell,n} - x_n - d$ is a space gap between two vehicles following each other; the subscript ℓ marks variables related to the preceding vehicle; $v_{s,n}$ is a safe speed at time step n; v_{free} is the free flow speed in free flow, all vehicles have the same length d; and $\widetilde{v}_{n+1}$ is the vehicle speed without speed fluctuations ξ_n:

$$\widetilde{v}_{n+1} = \min(v_{\text{free}}, v_{s,n}, v_{c,n}). \tag{6}$$

Model functions and parameters are given in Appendix A.

Simulations show that qualitative results related to the application in Fig. 1 are the same when rules of motion of automated vehicles in the model of mixed traffic are described either by the classical adaptive cruise control (ACC) model [26–31] or by a model for ACC in the framework of the three-phase traffic theory (called TPACC) [73]. For simplicity, we present only results of simulations of automated vehicle motion based on the classical ACC model that is equivalent to Helly's car-following model [79], in which acceleration $a^{(\text{AV})}$ of the automated vehicle is determined by the space gap to the preceding vehicle g and the relative speed $v_\ell - v^{(\text{AV})}$ measured by the automated vehicle as well as by a desired time headway $\tau_d^{(\text{AV})}$ of the automated vehicle to the preceding vehicle (see, e.g., Refs. [26–31]),

$$a^{(\text{AV})} = K_1\left(g - v^{(\text{AV})}\tau_d^{(\text{AV})}\right) + K_2\left(v_\ell - v^{(\text{AV})}\right), \tag{7}$$

where $v^{(\text{AV})}$ is the speed of the automated vehicle, v_ℓ is the speed of the preceding vehicle; here $v^{(\text{AV})}$, v_ℓ, and g are time functions; K_1 and K_2 are coefficients of automated vehicle adaptation. Because the model for human-driving vehicles

(4)–(6) is discrete in time, we simulate the model (7) with discrete time $n\tau$; the discrete version of the model (7) [73] is as follows [78]:

$$a_n^{(\mathrm{AV})} = K_1\left(g_n - v_n^{(\mathrm{AV})}\tau_d^{(\mathrm{AV})}\right) + K_2\left(v_{l,n} - v_n^{(\mathrm{AV})}\right), \quad (8)$$

$$v_{c,n}^{(\mathrm{AV})} = v_n^{(\mathrm{AV})} + \tau \max\left(-b_{\max}^{(\mathrm{AV})}, \min\left(\left\lfloor a_n^{(\mathrm{AV})}\right\rfloor, a_{\max}^{(\mathrm{AV})}\right)\right), \quad (9)$$

$$v_{n+1}^{(\mathrm{AV})} = \max\left(0, \min\left(v_{\mathrm{free}}, v_{c,n}^{(\mathrm{AV})}, v_{\mathrm{s},n}\right)\right), \quad (10)$$

$$x_{n+1} = x_n + v_{n+1}^{(\mathrm{AV})}\tau, \quad (11)$$

where the safe speed $v_{\mathrm{s},n}$ in (10) is the same as that for human-driving vehicles (4) and (6) (Appendix A) and acceleration and deceleration of the automated vehicle is limited by some maximum acceleration $a_{\max}^{(\mathrm{AV})}$ and maximum deceleration $b_{\max}^{(\mathrm{AV})}$, respectively. In (4) and (10), the speed $v_{\mathrm{free}} = v_{\mathrm{free}}^{(\mathrm{priority})}$ for the priority road and $v_{\mathrm{free}} = v_{\mathrm{free}}^{(\mathrm{secondary})}$ for the secondary road that are, respectively, the same ones as those for human-driving vehicles [60].

Models of the vehicle merging onto the priority road for human-driving vehicles and for automated vehicles (when the microscopic traffic prediction is not used) are given, respectively, in Appendixes B 1 and B 2.

D. Simulations of microscopic traffic situations

Because measurements of microscopic traffic situations for unsignalized intersections are not available, microscopic traffic situations have been simulated with the model for mixed traffic in Sec. II C. As qualitatively shown by the red dashed road region in Fig. 1(a), for the microscopic traffic prediction we have chosen only vehicles that locations x correspond to conditions

$$x_{\mathrm{ints}} - L_{\mathrm{data}} \leqslant x \leqslant x_{\mathrm{ints}} + L_{\mathrm{data}} \quad (12)$$

on the priority road and locations

$$x \geqslant x_{\mathrm{ints}} - L_{\mathrm{data}} \quad (13)$$

on the secondary road, where x_{ints} is the intersection location; in all simulations, we have used $L_{\mathrm{data}} = 0.3$ km [80]. Speeds $v(t_p)$ and locations $x(t_p)$ of vehicles that are within road regions (12) and (13) [red vehicles in Fig. 1(b)] are denoted, respectively, in accordance with formulas

$$v_{\mathrm{data}}(t_p) = v(t_p), \quad (14)$$

$$x_{\mathrm{data}}(t_p) = x(t_p). \quad (15)$$

In accordance with Sec. II A and the model of mixed traffic, time in the microscopic traffic prediction denoted by $t = \widetilde{t}_n$ is a discrete value

$$\widetilde{t}_n = t_p + n\tau, \ n = 0, 1, 2, \ldots \quad (16)$$

that satisfies conditions $t_p \leqslant \widetilde{t}_n \leqslant t_p + \Delta T_p$. Vehicle speeds (14) and locations (15) are used for the microscopic traffic prediction as the initial conditions related to $n = 0$ in (16):

$$x_n = x_{\mathrm{data}}(t_p), \ v_n = v_{\mathrm{data}}(t_p) \quad \text{at } n = 0. \quad (17)$$

Downstream of the red dashed road region in Figs. 1(b) and 1(c), speeds and locations of vehicles are found in the previous prediction [green colored vehicles in Fig. 1(b)].

III. PHYSICS OF MOTION OF AUTOMATED VEHICLE BASED ON MICROSCOPIC TRAFFIC PREDICTION

When no microscopic traffic prediction has applied, we use a well-known rule that the automated vehicle must stop at the intersection before turning right on the priority road [dashed curve in Fig. 2(a)]. A qualitative different case occurs when through the automated vehicle control based on the microscopic traffic prediction the automated vehicle can turn right onto the priority road without stopping at the road intersection [solid curve in Fig. 2(a)]. The physics of the microscopic traffic prediction is as follows.

(1) *The determination of time instant t_1 of the beginning of the prediction*. In the simulated scenario (Fig. 2), $t_1 = 57$ s (vertical red line t_1 in Fig. 2). This is because at this time instant the preceding vehicle labeled by i [Figs. 2(b) and 2(c)] has merged onto the priority road and, therefore, the following automated vehicle [black curves labeled by automated vehicle in Figs. 2(b) and 2(c)] can choose its deceleration freely while approaching the intersection [81].

(2) *The prediction of a pair of vehicles moving on the priority road between which the automated vehicle can merge without a stop at the intersection*. To find this pair of vehicles (these vehicles are labeled by numbers 5 and 6 in Figs. 2 and 3), safety conditions (3) should be satisfied in which

$$\tau^- = (s^- - d)/v^-, \quad \tau^+ = (s^+ - d)/v^{(\mathrm{AV})}, \quad (18)$$

where s^+ and s^- are gross space gaps between the automated vehicle and, respectively, the preceding vehicle (vehicle 5 in Fig. 3) and the following vehicle (vehicle 6 in Fig. 3); v^- is the speed of the following vehicle; all values in (18) are related to a predicted time instant $t = t_{\mathrm{E}}$ at which the automated vehicle can turn right at the intersection.

(3) *The prediction of time instant $t = t_{\mathrm{E}}$*. In addition to safety conditions (3), the choice of the pair of vehicles 5 and 6 should satisfy the following conditions (Fig. 3):

$$t_{\min} \leqslant t_{\mathrm{E}} < t_{\max}, \quad (19)$$

where $t_{\min}$ and $t_{\max}$ are predicted time instants at which the automated vehicle can reach the intersection moving, respectively, with maximum acceleration (and/or maximum speed) and with a safe speed coming to a stop at $t = t_{\max}$; obviously that $t_{\min}, t_{\mathrm{E}}, t_{\max} > t_1$.

(4) *The deceleration b_1 of the automated vehicle at time instant t_1 is calculated.* The condition for the calculation of b_1 is that the automated vehicle should reach the intersection at the predicted time instant t_{E}. Calculated deceleration b_1 at time instant $t_1 = 57$ s is used for the prediction of automated vehicle trajectory as shown in Fig. 4. However, in accordance with (2), deceleration b_1 of the automated vehicle at $t_1 = 57$ s is applied during time interval $t_1 \leqslant t < t_2$ only [Fig. 5(a)].

(5) *Repetition of the predictions of the automated vehicle trajectory made at each next time instant t_p, $p = 2, 3 \ldots$*. For each time instant t_p, the predicted time instant t_{E} and the associated predicted deceleration b_p are calculated. As follows from (9)–(11), the automated vehicle moves with deceleration b_p within a time interval (2) in accordance with

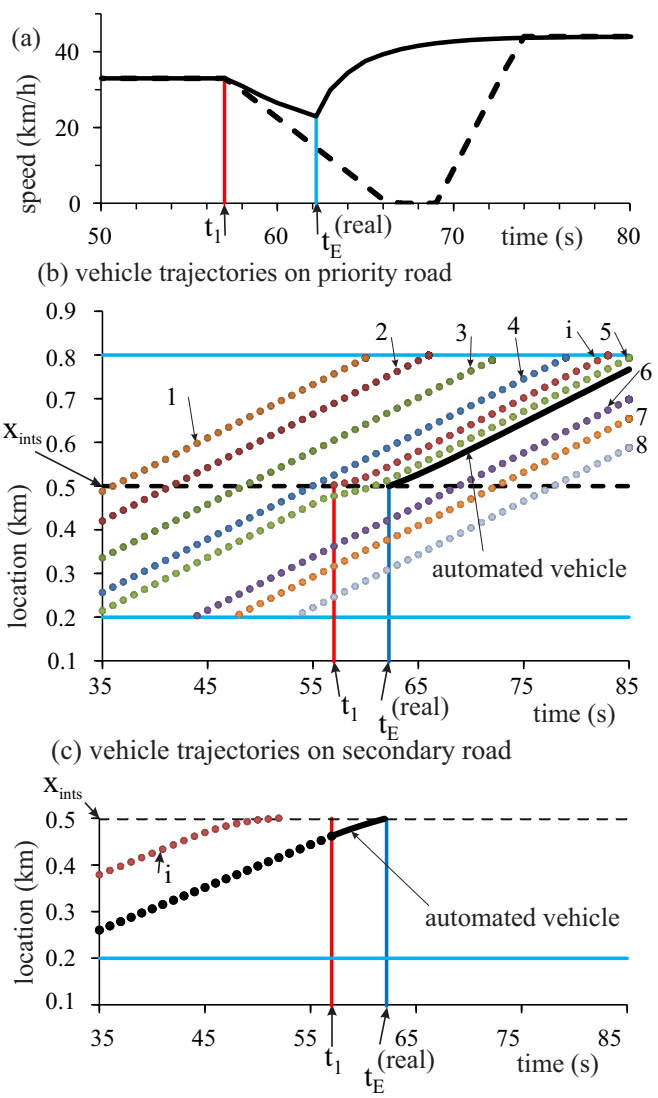

FIG. 2. Simulations of the motion of the automated vehicle with the use of the microscopic traffic prediction in accordance with the procedure of Fig. 1: (a) Time-dependencies of the speed of the automated vehicle controlled by the microscopic traffic prediction (solid curve) versus the speed of the automated vehicle without the use of the prediction (dashed curve). (b), (c) Vehicle trajectories on priority road (b) and secondary road (c); dotted curves: vehicle locations of simulated microscopic traffic situations, solid curve: trajectory of the automated vehicle controlled by the microscopic traffic prediction. $t_{\rm E}^{\rm (real)}$ is a time instant at which the automated vehicle really merges onto the priority road. Parameters of the model of human-driving vehicles are given in Table I of Appendix A; in (3), $\tau_1 = 2.0$ s and $\tau_2 = 0.5$ s; in (8)–(10), we have used $\tau_{\rm d}^{\rm (AV)} = 1.5$ s, $K_1 = 0.3$ s^{-2}, and $K_2 = 0.6$ s^{-1}; $a_{\rm max}^{\rm (AV)} = 2.5$ and $b_{\rm max}^{\rm (AV)} = 3\,{\rm m/s^2}$; all other parameters of the model of the automated vehicle are the same as those in Ref. [73]. A single-lane priority road is 2.5 km long; the intersection of this road with a single-lane secondary road that is 0.5 km long is at location $x_{\rm ints}$= 0.5 km; in mixed traffic flow, there are 1% of automated vehicles randomly distributed between human-driving vehicles. In simulations, the flow rate on the priority and secondary roads are, respectively, 1029 and 110 vehicles/h. Poisson distribution for entering vehicles has been used.

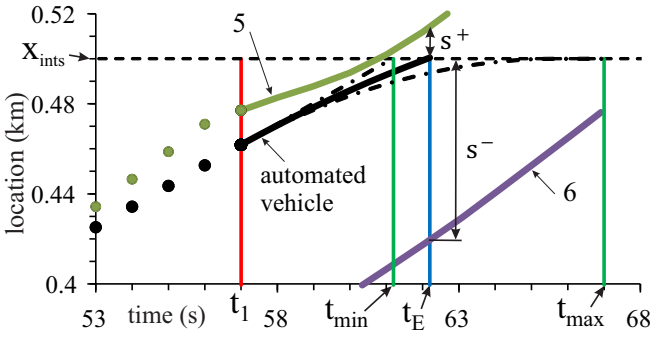

FIG. 3. Results of microscopic traffic prediction made for time instant $t_1 = 57$ s: Trajectories of vehicles 5 and 6 moving on the priority road between which the automated vehicle can merge at a predicted time instant $t_{\rm E}$ while satisfying conditions (3) and (19). Dotted parts of vehicle trajectories are related to real vehicle motion at $t \leqslant t_1 = 57$ s, solid parts of vehicle trajectories are predicted vehicle trajectories. Left and right dashed-dotted trajectories are virtual trajectories of the automated vehicle moving, respectively, with maximum acceleration (and/or maximum speed) and with a safe speed coming to a stop. $s^+ = g^+ + d$, $s^- = g^- + d$, where g^+ and g^- are the space gaps between the automated vehicle and the preceding vehicle (vehicle 5) and following vehicle (vehicle 6) at the predicted time instant $t_{\rm E}$, respectively. Calculated values $t_{\rm min} = 61.2$ s, $t_{\rm max} = 67$ s, $t_{\rm E} = 62.2$ s, $\tau^- = 6.27$ s, $\tau^+ = 1.02$ s. Other parameter designations, vehicle numbers, and model parameters are the same as those in Fig. 2.

equations

$$v_{c,n}^{\rm (AV)} = v_n^{\rm (AV)} + \tau \max\left(-b_{\rm max}^{\rm (AV)}, \min\left(-b_p,\ a_{\rm max}^{\rm (AV)}\right)\right), \quad (20)$$

$$v_{n+1}^{\rm (AV)} = \max\left(0, \min\left(v_{\rm free},\ v_{c,n}^{\rm (AV)}\right)\right), \quad (21)$$

and (11). The automated vehicle motion with deceleration b_p is only valid until the next traffic prediction for b_{p+1} is available at $t = t_{p+1}$. Then, during time interval $t_{p+1} \leqslant t < t_{p+2}$ the vehicle moves with Eqs. (20), (21), and (11) in which instead of the value b_p the predicted deceleration b_{p+1} is used, and so on.

In simulations of the microscopic traffic prediction, we choose $\delta t = t_{p+1} - t_p = \tau$, respectively, time instants t_p (1) at which the microscopic traffic prediction is made can be written as

$$t_p = t_1 + (p-1)\tau,\ \ p = 1, 2, \ldots, p_{\rm E}. \quad (22)$$

The repetition of the predictions of the automated vehicle trajectory is made up to some maximum time instant t_p denoted in (22) by $t_p = t_{p_{\rm E}}$. Conditions for the maximum time instant $t_p = t_{p_{\rm E}}$ and for the related time instant denoted by $t_{\rm E}^{\rm (real)}$ at which the automated vehicle really merges onto the priority road are presented in Appendix C.

At $t \geqslant t_{p_{\rm E}}$ the automated vehicle decelerates with the last predicted deceleration (Sec. C 1 of Appendix C) moving up to the road intersection at which it turns right onto the priority road; later, no prediction is made. In the simulated scenario (Fig. 2), it has been found that $p_{\rm E} = 6$ ($t_{p_{\rm E}} = 62$ s) and $t_{\rm E}^{\rm (real)} = 62.2$ s.

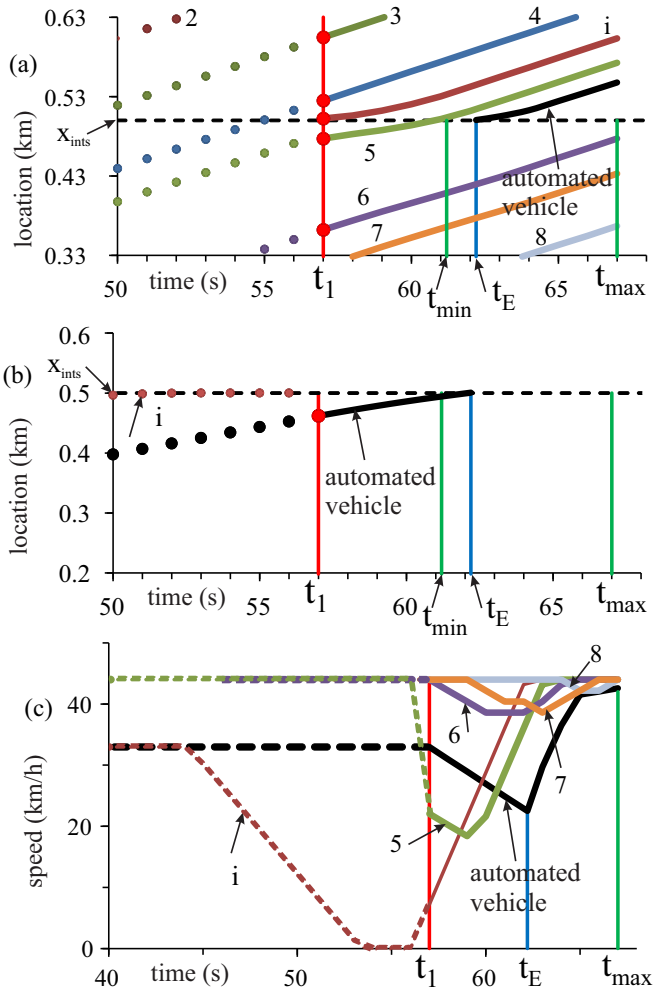

FIG. 4. Simulations of control of the automated vehicle through the use of the microscopic traffic prediction made for time instant $t_1 = 57$ s: (a), (b) Vehicle trajectories on priority (a) and secondary roads (b); dotted parts of trajectories—real vehicle motion, solid parts of trajectories—predicted vehicle motion. (c) Predicted vehicle speeds, dashed parts of trajectories—real vehicle motion, solid parts of trajectories—predicted vehicle motion. In (c), the predicted speed of the automated vehicle at time instant $t_E = 62.2$ s is equal to $v^{(AV)} = 22.5$ km/h. Other parameter designations, vehicle numbers, and model parameters are the same as those in Fig. 2.

A dependence of predicted values on t_p is illustrated in Fig. 5. Predicted decelerations b_2 at $t_2 = 58$ s and b_3 at $t_3 = 59$ s [Figs. 5(b) and 5(c)] are only applied by the automated vehicle control during time intervals $t_2 \leqslant t < t_3$ and $t_3 \leqslant t < t_4$, respectively. This explains why the automated vehicle deceleration can be a complex time function within time interval $t_1 \leqslant t \leqslant t_E^{(real)}$ [Fig. 5(d)].

The model of the calculation of the predicted time instant t_E is as follows. Conditions at which the automated vehicle can merge onto the priority road are

$$\tilde{g}^{+}_{n,m} \geqslant v^{+}_{n}\,\tau_2, \tag{23}$$

$$\tilde{g}^{-}_{n,m} \geqslant v^{-}_{n}\,\tau_1, \tag{24}$$

$$t_{\min} \leqslant \tilde{t}_{n,m} < t_{\max}, \tag{25}$$

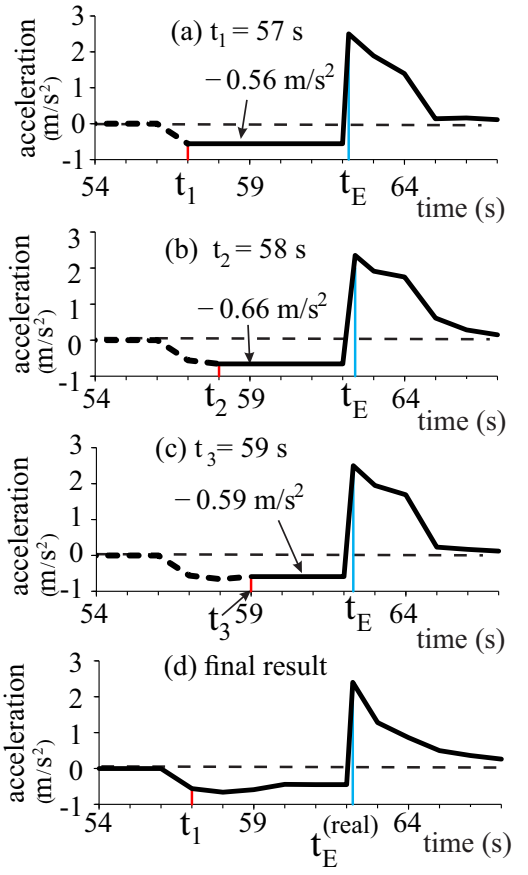

FIG. 5. Predicted automated vehicle decelerations [solid parts of curves in (a)–(c)] for $p = 1$ ($t_1 = 57$ s), $t_E = 62.2$ s, $b_1 = 0.56$ m/s^2 (a), for $p = 2$ ($t_2 = 58$ s), $t_E = 62.4$ s, $b_2 = 0.66$ m/s^2 (b), and for $p = 3$ ($t_3 = 59$ s), $t_E = 62.3$ s, $b_3 = 0.59$ m/s^2 (c). In (d), the final time function of the acceleration (deceleration) of the automated vehicle is shown; $t_E^{(real)} = 62.2$ s. Parameter designations, vehicle numbers, and model parameters are the same as those in Fig. 2.

where

$$\tilde{g}^{+}_{n,m} = \tilde{x}^{+}_{n,m} - x_{\text{ints}} - d, \tag{26}$$

$$\tilde{g}^{-}_{n,m} = x_{\text{ints}} - \tilde{x}^{-}_{n,m} - d, \tag{27}$$

$$\tilde{x}^{+}_{n,m} = x^{+}_{n-1} + v^{+}_{n}\, m\Delta\tau, \quad m = 1, 2, \ldots, M, \tag{28}$$

$$\tilde{x}^{-}_{n,m} = x^{-}_{n-1} + v^{-}_{n}\, m\Delta\tau, \quad m = 1, 2, \ldots, M, \tag{29}$$

$\Delta\tau = 0.1\tau = 0.1$ s, $M = \tau/\Delta\tau = 10$, the time $\tilde{t}_{n,m}$ in (25)

$$\tilde{t}_{n,m} = \tilde{t}_{n-1} + m\,\Delta\tau, \quad m = 1, 2, \ldots, M \tag{30}$$

describes the discrete time with short time step $\Delta\tau$ within a time interval between $\tilde{t}_{n-1}$ and $\tilde{t}_n$ (16), where n =1,2,...; superscripts + and – denote, respectively, the preceding and following vehicles on the priority road with respect to the intersection location x_{ints}. Conditions (23) and (24) correspond to (3). The predicted time instant t_E is found as

$$t_E = \min_{n,m}(\tilde{t}_{n,m}), \tag{31}$$

where (31) is calculated under conditions (23)–(25).

To find the minimum value (31), the speeds and locations of vehicles on the main road [Figs. 1(b) and 1(c)] are calculated at subsequent time moments $\widetilde{t}_n$ within interval $t_{\min} \leqslant \widetilde{t}_n < t_{\max}$. At time $\widetilde{t}_n$ it is proven whether there is a pair of consequent vehicles on the main road for which conditions (23)–(25) are satisfied at some index m. If yes, the value $m_{\rm E} = m$ for which $\widetilde{t}_{n,m}$ in (31) reaches a minimum is found, indexes $n_{\rm E} = n - 1$ and $m_{\rm E} = m$ are stored, and $t_{\rm E}$ is found from (30) as

$$t_{\rm E} = \widetilde{t}_{n_{\rm E}} + m_{\rm E}\Delta\tau. \tag{32}$$

If there is no pair of consequent vehicles on the main road for which conditions (23)–(25) are satisfied, calculations are repeated for the next time step $\widetilde{t}_{n+1}$, if condition $\widetilde{t}_{n+1} < t_{\max}$ is satisfied, and so on. Note that conditions (23) and (24) guarantee that at the predicted time instant $t_{\rm E}$ the first vehicle in the pair of consequent vehicles is downstream of the intersection and the second one is upstream of the intersection. If no time $t_{\rm E}$ can be found from the above procedure of the microscopic traffic prediction, the automated vehicle decelerates with the safe speed to come to a stop at the intersection. The model for the prediction of $t_{\min}$, $t_{\max}$, and $b_{\rm p}$ is presented in Appendix C.

The use of the microscopic traffic prediction leads to a speed harmonization in city traffic (Fig. 6). Through the use of the prediction, the speeds of vehicles 7 and 8 following the automated vehicle increase considerably [Fig. 6(b)] in comparison with the case when no traffic prediction is used [Fig. 6(c)].

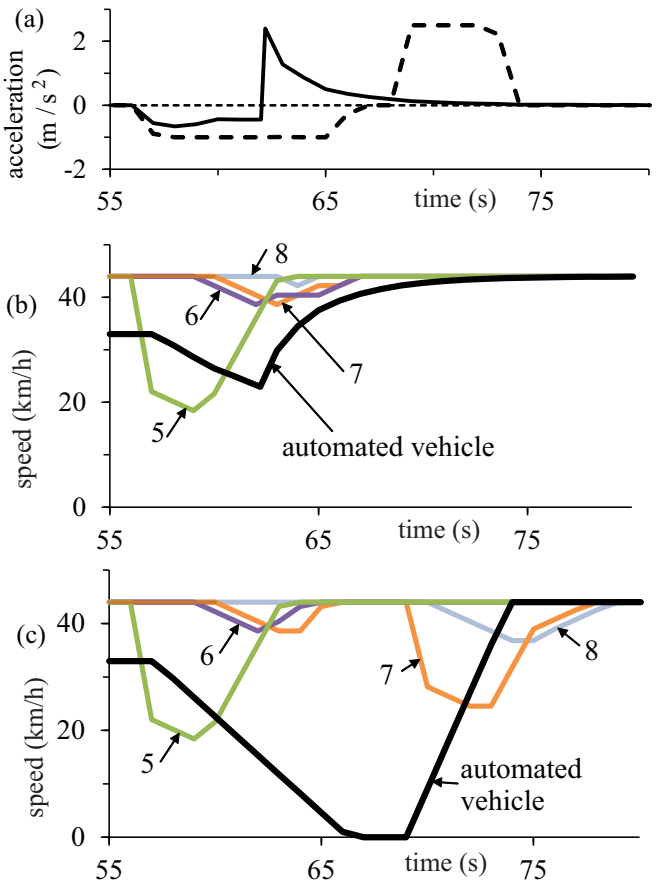

FIG. 6. Speed harmonization through the use of the microscopic prediction: (a) Automated vehicle acceleration under the use of the prediction (solid curve) versus the case when no prediction is used (dashed curve). (b), (c) Time dependencies of vehicle speeds under the use of the prediction (b) versus the case when no prediction is used (c). Vehicle numbers and model parameters are the same as those in Fig. 2.

IV. EFFECT OF UNCERTAINTY IN DATA USED FOR MICROSCOPIC TRAFFIC PREDICTION

In Sec. III, we have assumed that vehicle speeds and locations in microscopic traffic situations that are used as initial conditions for the microscopic traffic prediction at time instants t_p (22) have no errors in comparison with real vehicle speeds and locations of microscopic traffic situations [dotted parts of trajectories in Figs. 2(b), 2(c) 3, 4(a), and 4(b)]. In reality, there can be data latency errors and/or random errors in measurements of the vehicle speeds and locations in microscopic traffic situations used in the microscopic traffic prediction. We can call the errors the uncertainty of traffic data used in the prediction model (Fig. 1). We assume that there should be some maximum amplitude of random errors in measurements of the vehicle speeds and/or vehicle locations that depend on the measurement technology.

A. Data latency

There can be a latency between the data of microscopic traffic situations and the data used in the prediction model (Fig. 1) at time instants t_p (22). The latency denoted by $\tau_{\rm lat}$ (Fig. 7) can be caused by a delay in the procedure of data measurements and the data transfer; in this case, we can assume that $\tau_{\rm lat}$ is a constant value, $\tau_{\rm lat} \leqslant \tau$. The following initial conditions are used when there is a latency in the data used in the prediction model:

$$x_n = x_{\rm data}(t_{\rm p}),\ v_n = v_{\rm data}(t_{\rm p}) \quad \text{at } n = 0, \tag{33}$$

where

$$x_{\rm data}(t_{\rm p}) = x(t_{\rm p}) - v(t_{\rm p})\tau_{\rm lat}, \tag{34}$$

$$v_{\rm data}(t_{\rm p}) = v(t_{\rm p}) - (v(t_{\rm p}) - v(t_{\rm p} - \tau))\tau_{\rm lat}/\tau. \tag{35}$$

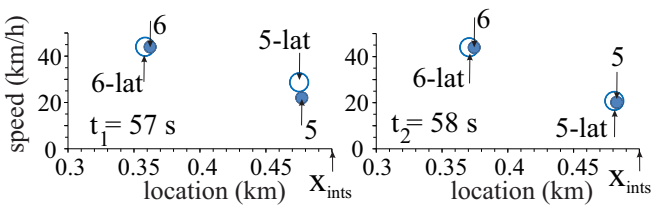

FIG. 7. Speeds and locations of vehicles 5 and 6 in data of microscopic traffic situations without data uncertainty (color-filled circles labeled by 5 and 6) and under a latency in the data (empty circles labeled by 5-lat and 6-lat) at two subsequent time instants $t_1 = 57$ s (left) and $t_2 = 58$ s (right) at which the microscopic traffic prediction is calculated. Latency $\tau_{\rm lat} = 0.3$ s. Vehicle numbers and other model parameters are the same as those in Fig. 2.

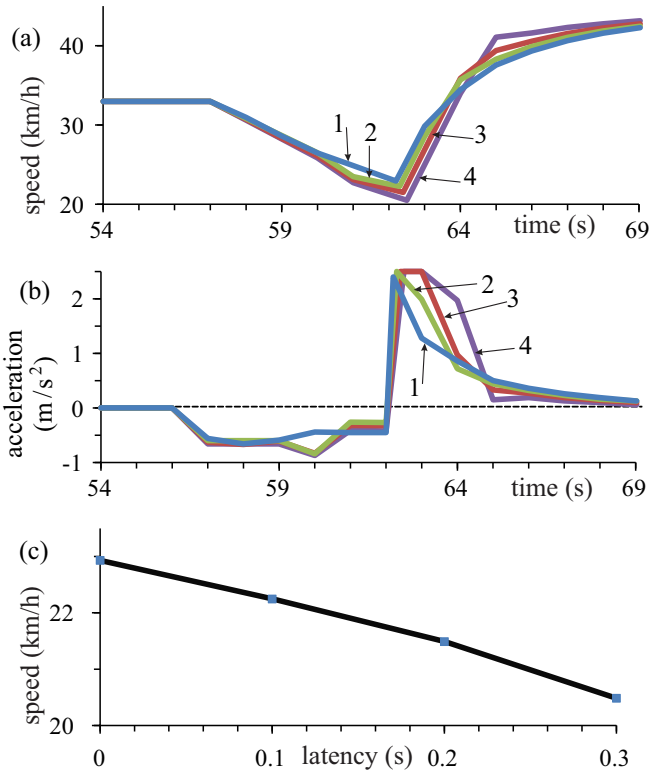

FIG. 8. Effect of data latency τ_{lat} on the microscopic traffic prediction of the automated vehicle speed (a) and acceleration (b) for the case of microscopic traffic situations used in Sec. III (Figs. 2–6): $\tau_{lat} = 0$ for curves 1, $\tau_{lat} = 0.1$ s for curves 2, $\tau_{lat} = 0.2$ s for curves 3, and $\tau_{lat} = 0.3$ s for curves 4; curves 1 for $\tau_{lat} = 0$ are, respectively, the same as those given for the automated vehicle by solid curves in Figs. 2(a) and 5(d). (c) Data-latency-function of the speed of the automated vehicle $v^{(AV)}$ at time instant $t = t_E^{(real)}$.

Simulations show (Fig. 8) that with the increase in the data latency the minimum speed at which the automated vehicle merges onto the priority road through the application of the prediction decreases [Fig. 8(c)]. However, even for latency $\tau_{lat} = 0.3$ s the minimum speed remains relatively high: By $\tau_{lat} = 0$ and 0.3 s, the minimum speeds are equal about to 22.9 km/h [curve 1 in Fig. 8(a)] and 20.5 km/h [curve 4 in Fig. 8(a)], respectively.

B. Random errors in vehicle locations

The data uncertainty can be caused by random errors in vehicle locations in the data of microscopic traffic situations (Fig. 9). We assume that the errors are independent of each other and they are described by formula $\rho\Delta x$, where $\rho = \text{rand}(-1, 1)$ is a random number uniformly distributed between -1 and 1. Here Δx is a maximum amplitude of the errors that is assumed to be a constant value.

Random errors in vehicle locations in the data of microscopic traffic situations lead to very complex vehicle trajectories of all vehicles with the exception of the automated vehicle trajectory (Fig. 10). This is because the automated vehicle is controlled through the use of the microscopic traffic prediction.

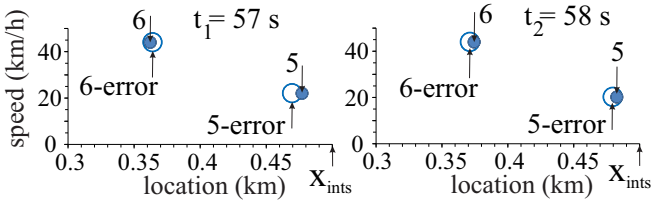

FIG. 9. Speeds and locations of vehicles 5 and 6 without data uncertainty (color-filled circles labeled by 5 and 6) and under data uncertainty caused by random errors in vehicle locations (empty circles labeled by 5-error and 6-error) at two subsequent time instants $t_1 = 57$ s (left) and $t_2 = 58$ s (right) at which the microscopic traffic prediction is calculated. Amplitude of random errors is $\Delta x = 10$ m. Vehicle numbers and other model parameters are the same as those in Fig. 2.

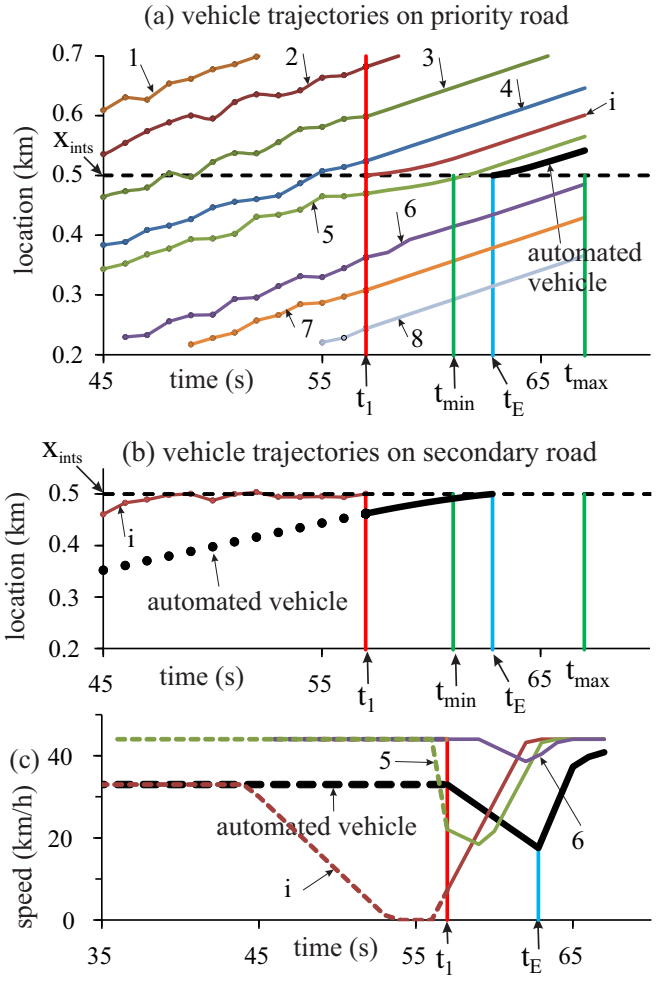

FIG. 10. Simulations of the automated vehicle control with the use of the microscopic traffic prediction calculated at $t_1 = 57$ s in accordance with the procedure of Fig. 1 under data uncertainty caused by random errors in vehicle locations in the data of microscopic traffic situations: (a), (b) Vehicle trajectories on priority road (a) and secondary road (b). (c) The time-dependencies of microscopic vehicle speeds of some vehicles. $\Delta x = 10$ m. Calculated values $t_{min} = 61.1$ s, $t_E = 62.8$ s, $t_{max} = 67$ s. Vehicle numbers and other model parameters are the same as those in Fig. 2.

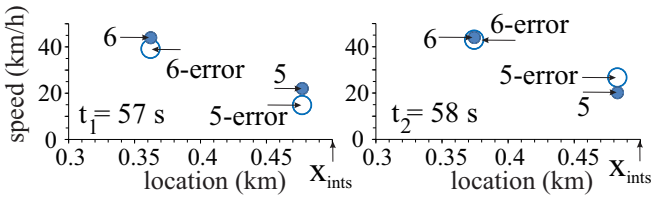

FIG. 11. Speeds and locations of vehicles 5 and 6 without data uncertainty (color filled circles labeled by 5 and 6) and under data uncertainty caused by random errors in vehicle speeds (empty circles labeled by 5-error and 6-error) at two subsequent time instants $t_1 = 57$ s (left) and $t_2 = 58$ s (right) at which the microscopic traffic prediction is calculated. $\Delta v = 3$ m/s. Vehicle numbers and other model parameters are the same as those in Fig. 2.

C. Random errors in vehicle speeds

The data uncertainty can be caused by errors in vehicle speeds in the data of microscopic traffic situations (Fig. 11). As in Sec. IV B, we assume that the random errors in the vehicle speeds can be described by formula $\rho\Delta v$, where $\rho = \text{rand}(-1, 1)$ is a random number uniformly distributed between -1 and 1, Δv is a maximum amplitude of the errors. Random errors in vehicle speeds in the data of microscopic traffic situations lead to very complex behavior of the speed of all vehicles with the exception of the automated vehicle trajectory that is controlled through the use of the microscopic traffic prediction (Fig. 12).

D. Initial conditions for prediction under errors in data of microscopic traffic situations

The following initial conditions for the microscopic traffic prediction are used when there are errors in the data of microscopic traffic situations:

$$v_n = \max\left(0, \min\left(v_{\text{free}}, v_{\text{data}}(t_{\text{p}})\right)\right) \quad \text{at } n = 0, \tag{36}$$

$$x_n = \min\left(x_{\text{data}}(t_{\text{p}}), x_{\ell,n} - v_n\tau - d\right) \text{ at } n = 0, \tag{37}$$

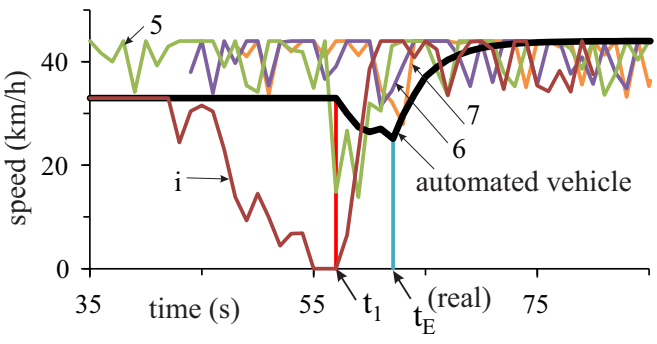

FIG. 12. Simulations of the automated vehicle control based on the microscopic traffic prediction in accordance with the procedure of Fig. 1, when data uncertainty is caused by random errors in vehicle speeds in the data of microscopic traffic situations: The time dependencies of microscopic vehicle speeds of some vehicles. $\Delta v = 3$ m/s. Calculated value $t_{\text{E}}^{(\text{real})} = 62.1$ s. Vehicle numbers and other model parameters are the same as those in Fig. 2.

where, under random errors in locations of vehicles within road regions (12) and (13) (Sec. IV B), in accordance with (22), x_{data} are found from formulas

$$x_{\text{data}}(t_p) = x(t_p) + \rho\Delta x, \;\; p = 1, 2, \ldots, p_{\text{E}}, \tag{38}$$

respectively, under random errors in speeds of vehicles within road regions (12) and (13) (Sec. IV B), v_{data} are found from formulas

$$v_{\text{data}}(t_p) = v(t_p) + \rho\Delta v, \;\; p = 1, 2, \ldots, p_{\text{E}}. \tag{39}$$

Equations (36) and (37) determine physical limitations for the application of random errors in speeds and locations of vehicles (38) and (39) in simulations: (i) the speed should satisfy conditions $0 \leqslant v_n \leqslant v_{\text{free}}$ (36) and (ii) the space gap to the preceding vehicle cannot be less than some safety gap that is chosen as $v_n\tau$ in (37).

V. STOCHASTIC FEATURES OF MICROSCOPIC TRAFFIC PREDICTION UNDER UNCERTAINTY IN DATA

A. Set of realizations of microscopic traffic prediction

Due to a random character of errors in vehicle locations (and/or speeds) in the data of a microscopic traffic situation for a particular time instant t_p, the associated microscopic traffic prediction can be considered a *random realization* of the microscopic traffic prediction (automated vehicle control with the use of such a random realization of the microscopic traffic prediction made at $t_p = t_1$ is shown in Fig. 10).

During the whole time interval of the automated vehicle control beginning at $t = t_1$, there is a sequence of time instants t_p (22) at which different microscopic traffic situations are available and, respectively, the microscopic traffic predictions are repeated (Sec. II A). Therefore, there is a sequence of random realizations of the microscopic traffic predictions made at different t_p (22), which can be considered a *set of the realizations* of the microscopic traffic prediction.

In accordance with Sec. II A, the set of the realizations of the microscopic traffic prediction can be considered to be successful only when safety conditions (3) are satisfied for *each* of the realizations of the set. It must be stressed that values τ^+ and τ^- in (3) are related to gross space gaps s^+ and s^- (18) between the automated vehicle and the preceding and following vehicles (respectively, vehicles 5 and 6 in Fig. 3) found *without any data uncertainty* as considered in Figs. 2–6. The microscopic traffic situations without any data uncertainty can be considered *real data* of microscopic traffic situations.

In a study presented in Figs. 2–6, no errors in the data of microscopic traffic situations have been assumed. In the same traffic scenario, under errors in the data, real data of microscopic traffic situations are *not known* by the calculation of the microscopic traffic prediction. Therefore, rather than (3), the following safety conditions have to be used:

$$\tau^-_{\text{error}} \geqslant \tau_1, \;\; \tau^+_{\text{error}} \geqslant \tau_2, \tag{40}$$

where

$$\tau^-_{\text{error}} = (s^-_{\text{error}} - d)/v^-, \;\; \tau^+_{\text{error}} = (s^+_{\text{error}} - d)/v^{(\text{AV})}, \tag{41}$$

s^-_{error}, s^+_{error} and τ^-_{error}, τ^+_{error} are, respectively, gross space gaps and time headway of the automated vehicle to the following

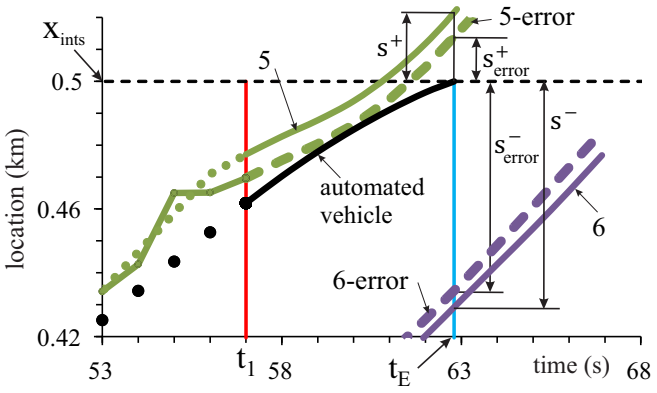

FIG. 13. Continuation of Fig. 10: Parts of some vehicle trajectories that numbers 5, 6 in Fig. 10 are replaced here by, respectively, 5-error, 6-error, and associated gross space gaps $s^+_{\rm error}$, $s^-_{\rm error}$ with errors. Trajectories of vehicles 5 and 6 with no errors are taken from Fig. 3.

and preceding vehicles at $t = t_{\rm E}$ *with errors*, which (as the speeds v^- and $v^{(\rm AV)}$) are calculated from the microscopic traffic prediction in which microscopic traffic situations with random errors have been used (trajectories 5-error and 6-error in Fig. 13).

B. Physical limitation of the applicability of microscopic traffic prediction

The microscopic traffic prediction can be used for the automated vehicle control only, when for each of the time instants from the sequence of time instants t_p (22) safety conditions (3) are satisfied. Otherwise, the microscopic traffic prediction cannot be *reliably* used for the automated vehicle control.

Thus, for a reliable application of the microscopic traffic prediction, we should be sure that when safety conditions (40) are satisfied for the predicted time headway $\tau^+_{\rm error}$ and $\tau^-_{\rm error}$ at each of the time instants t_p (22), then also safety conditions (3) are satisfied for real time headway τ^+ and τ^+ [82].

In Figs. 2–6, in which no errors in the data of microscopic traffic situations have been assumed, gross space gaps s^+, s^- correspond to *real* values of the gross space gaps. It should be emphasized that under errors in the data of microscopic traffic situations, gross space gaps with errors $s^+_{\rm error}$, $s^-_{\rm error}$ can differ considerably, respectively, from real gross space gaps s^+, s^-. This can be seen from Fig. 13. Nevertheless, as shown in Fig. 14 (solid curves), safety conditions (3) are satisfied for each of the time instants from the sequence of time instants t_p (22); therefore, the set of realizations (called set 1 below) is applicable for the automated vehicle control.

As mentioned, in Figs. 2–6, no errors in the data of microscopic traffic situations have been assumed. In the same traffic scenario, very different random errors in the data of microscopic traffic situations can occur. This causes many different sets of the random realizations of the microscopic traffic prediction (strictly speaking, the infinite number of sets). Therefore, in addition to set 1 (Fig. 14), we have studied another set of the random realizations of the microscopic traffic prediction denoted by set 2 (Fig. 15): Random errors in the data of microscopic traffic situations in set 2 are different

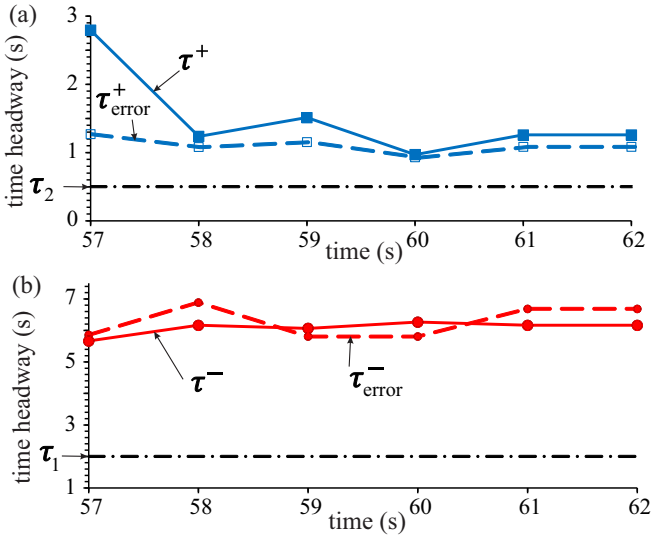

FIG. 14. Simulations of safety conditions (3) and (40) during the time of the microscopic traffic prediction as functions of time instants t_p (22) for a set of realizations that is denoted by set 1: (a) Time headway τ^+ (solid curve) and $\tau^+_{\rm error}$ (dashed curve). (b) Time headway τ^- (solid curve) and $\tau^-_{\rm error}$ (dashed curve). In (22), $p_{\rm E} = 6$. Time headway τ^+, τ^- are given by (18) and time headway $\tau^+_{\rm error}$, $\tau^-_{\rm error}$ are given by (41). Data for $t_1 = 57$ s are related to Figs. 10 and 13.

from those in set 1 (Fig. 14). It has been found that under the same scenario as that used in set 1, in set 2 it occurs that even when safety conditions (40) used by the microscopic traffic prediction are satisfied for each of the time instants t_p (22)

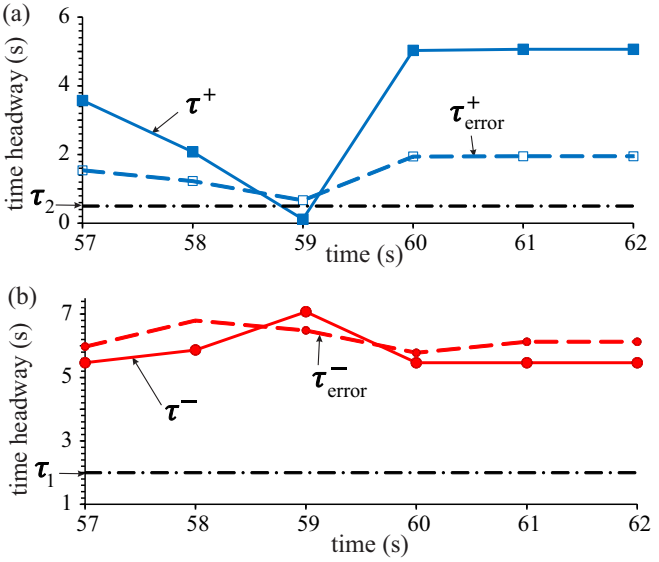

FIG. 15. Simulations of safety conditions (3) and (40) for another set of realizations denoted by set 2 during the time of the microscopic traffic prediction as functions of time instants t_p (22) under errors with $\Delta x = 10$ m in vehicle locations in the data of microscopic traffic situations: (a) Time headway τ^+ (solid curve) and $\tau^+_{\rm error}$ (dashed curve). (b) Time headway τ^- (solid curve) and $\tau^-_{\rm error}$ (dashed curve). In (22), $t_1 = 57$ s and $p_{\rm E} = 6$. Time headway τ^+, τ^- are given by (18) and time headway $\tau^+_{\rm error}$, $\tau^-_{\rm error}$ are given by (41).

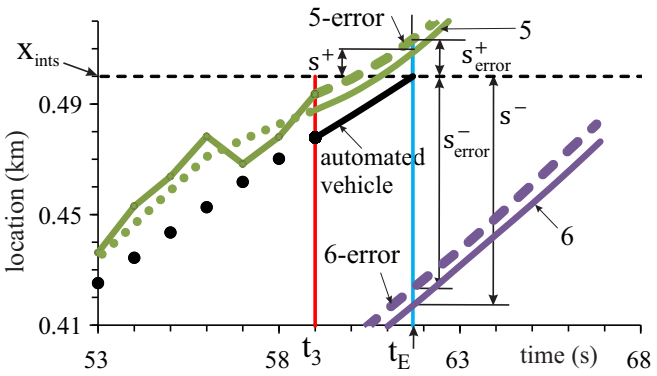

FIG. 16. Parts of vehicle trajectories 5-error and 6-error with errors and the associated gross space gaps s^+_{error}, s^-_{error} related to set 2 of realizations shown in Fig. 15 for time instant $t_3 = 59$ s. Trajectories 5 and 6 are vehicle trajectories with no errors, taken from Fig. 3.

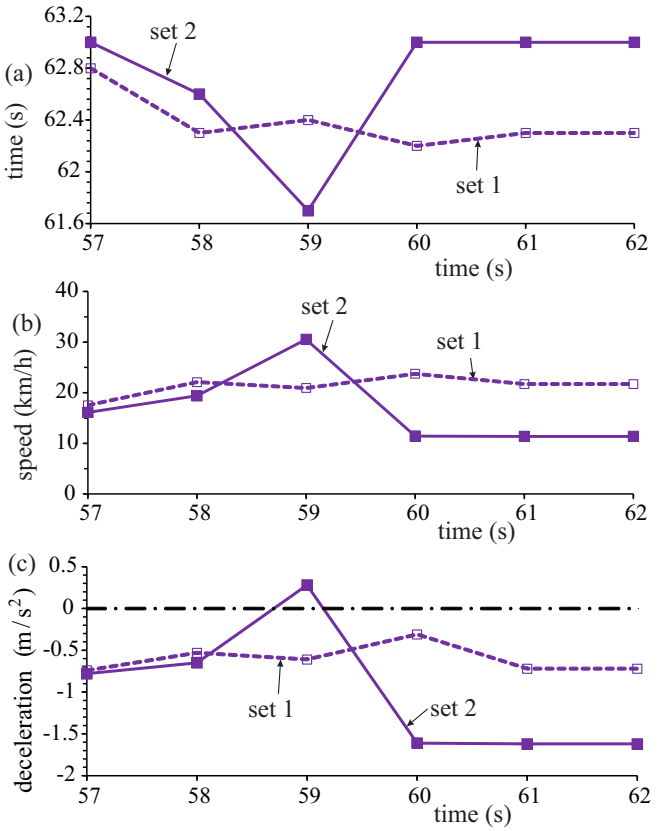

FIG. 17. Simulations of stochastic features of microscopic traffic prediction under errors in vehicle locations in the data of microscopic traffic situations. $\Delta x = 10$ m. Comparison of predicted time instants of automated vehicle merging t_E (a), predicted automated vehicle speed $v^{(AV)}$ by the merging (b), and predicted automated vehicle deceleration (acceleration) (c) as functions of time instants t_p (22) for two sets of realizations: dashed curves set 1 and solid curves set 2 are related to Figs. 14 and 15, respectively. In (22), $t_1 = 57$ s and $p_E = 6$.

(dashed curves in Fig. 15), nevertheless, safety conditions (3) fail for one of the time instants t_p (22); this case is realized for $t_3 = 59$ s [value $\tau^+(t_3) = 0.12$ s is shorter than $\tau_2 = 0.5$ s]. Therefore, in this case (set 2), the prediction cannot be reliably applied for the automated vehicle control.

To understand the failure of safety conditions (3) for set 2 of random realizations at $t_3 = 59$ s (Fig. 15), we compare Figs. 13 and 16. In Fig. 13, the predicted space gap s^+_{error} between the preceding vehicle 5 and the automated vehicle by the merging becomes *shorter* than the real space gap s^+. As a result, in set 1 when safety conditions (40) are satisfied, then conditions (3) are also satisfied; this result remains true for all other time instants t_p (22) (Fig. 14). Contrarily, for set 2 of realizations, the predicted gap s^+_{error} at $t_p = t_3 = 59$ s becomes longer than the real space gap s^+ (Fig. 16); for this reason, although conditions (40) are satisfied, however, safety conditions (3) are not satisfied for set 2 (Fig. 15).

This result correlates with the behavior of characteristics of the microscopic traffic prediction (Fig. 17): Predicted time instants of automated vehicle merging t_E, predicted automated vehicle speed $v^{(AV)}$ by the merging, and predicted automated vehicle deceleration (acceleration) as functions of time instants t_p (22) are, respectively, totally different (Fig. 17) for the two sets of realizations shown in Figs. 14 and 15. Sometimes, after a deceleration at some time instant t_p, the automated vehicle should accelerate at the next time instant t_{p+1} to turn right at the intersection without the stop [see, e.g., $t_p = t_2 = 58$ s and $t_{p+1} = t_3 = 59$ s on curve set 2 in Fig. 17(c)]. This also explains different time dependencies of the automated vehicle speed [Fig. 18(a)] and acceleration (deceleration) [Fig. 18(b)] related to automated vehicle control with the use of two different sets of realizations.

These results remain qualitatively the same when the data uncertainty is caused by errors in vehicle speeds (Figs. 19 and 20). For the first set of realizations (Fig. 19), safety conditions (3) are satisfied for each of the time instants t_p (22). Thus, the first set of realizations (Fig. 19) can be used for the automated vehicle control. Contrarily, for the second set of realizations (Fig. 20), safety conditions (3) are *not* satisfied for $t_p = t_2 = 58$ s: value $\tau^+(t_2) = 0.26$ s is shorter than $\tau_2 = 0.5$ s. Therefore, in this case (Fig. 20), the prediction cannot be reliably applied for the automated vehicle control.

We have found that the effect of the data uncertainty on the stochastic features of the microscopic traffic prediction for automated driving remains qualitatively the same when the data uncertainty is caused a combination of errors in vehicle locations and speeds. For this reason, below, to derive other general qualitative conclusions about the effect of the data uncertainty on the stochastic features of the microscopic traffic prediction, we can limit by a consideration of the errors in vehicle locations in the data of microscopic traffic situations.

As mentioned, there can be an infinite number of different sets of realizations associated with random errors in the data of microscopic traffic situations. Therefore, there can be a set of realizations of the microscopic traffic prediction for which safety conditions (3) fail at least for some of the time instants t_p (22), contrarily, safety conditions (40) are satisfied for each of the time instants t_p (22). This effect causes a basic physical limitation of the applicability of the microscopic traffic prediction for the automated vehicle control.

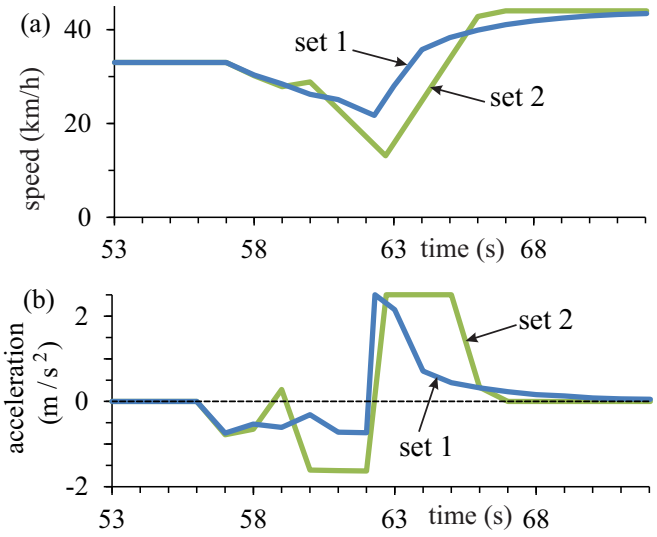

FIG. 18. Simulations of stochastic features of microscopic traffic prediction under errors in vehicle locations in the data of microscopic traffic situations. $\Delta x = 10$ m. Comparison of the speed (a) and deceleration (acceleration) (b) of the automated vehicle that is controlled based on two different microscopic traffic predictions associated with sets of realizations 1 and 2: curves set 1 and curves set 2 are related to Figs. 14 and 15, respectively.

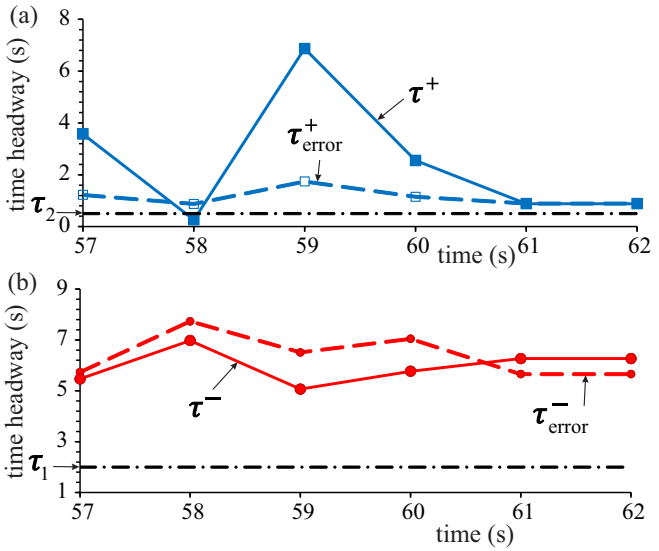

FIG. 20. Simulations of safety conditions (3) and (40) as functions of t_p (22) for another set of realizations of the microscopic traffic prediction that is denoted by *second set* under errors with $\Delta v = 3$ m/s in vehicle speeds in the data of microscopic traffic situations: (a) Time headway τ^+ (solid curve) and τ^+_{error} (dashed curve). (b) Time headway τ^- (solid curve) and τ^-_{error} (dashed curve). In (22), $t_1 = 57$ s and $p_{\text{E}} = 6$. Time headway τ^+, τ^- are given by (18) and time headway τ^+_{error}, τ^-_{error} are given by (41).

VI. PROBABILISTIC DESCRIPTION OF MICROSCOPIC TRAFFIC PREDICTION

A. Critical uncertainty in data

Simulations show that when there is no uncertainty in the data of microscopic traffic situations, safety conditions (3) of the applicability of the microscopic traffic prediction for the traffic scenario presented in Figs. 2–6 (Sec. III) are always satisfied. However, in the same traffic scenario under uncertainty in measured data of microscopic traffic situations at least for some time instants t_p (22) safety conditions (3) can fail (Figs. 15 and 20). Therefore, for each particular traffic situation, in which the microscopic traffic prediction is applied for automated driving, there should be some *critical uncertainty* for the applicability of the microscopic traffic prediction. We denote the critical uncertainty by $\Delta x = \Delta x_{\text{cr}}$ in the case of errors in vehicle locations in the data of microscopic traffic situations and by $\Delta v = \Delta v_{\text{cr}}$ in the case of errors in vehicle speeds in the data.

The physical sense of the critical uncertainty is as follows: When the uncertainty in the data of microscopic traffic situations is equal to or less than the critical uncertainty ($\Delta x \leqslant \Delta x_{\text{cr}}$ or $\Delta v \leqslant \Delta v_{\text{cr}}$), then the microscopic traffic prediction can be reliably applied for automated driving in the particular traffic situation. Otherwise, when the uncertainty in the data of microscopic traffic situations is larger than the critical uncertainty ($\Delta x > \Delta x_{\text{cr}}$ or $\Delta v > \Delta v_{\text{cr}}$), then the microscopic traffic prediction cannot be considered as a reliably applicable for the particular traffic situation.

To understand the definition of the critical uncertainty, we should mention that the reliable application of the microscopic traffic prediction for automated vehicle control can only be ensured, if for any set of realizations safety conditions (3) are satisfied for each of the time instants t_p (22) at which the microscopic traffic prediction is applied. This is realized when data uncertainty does not exceed the critical uncertainty.

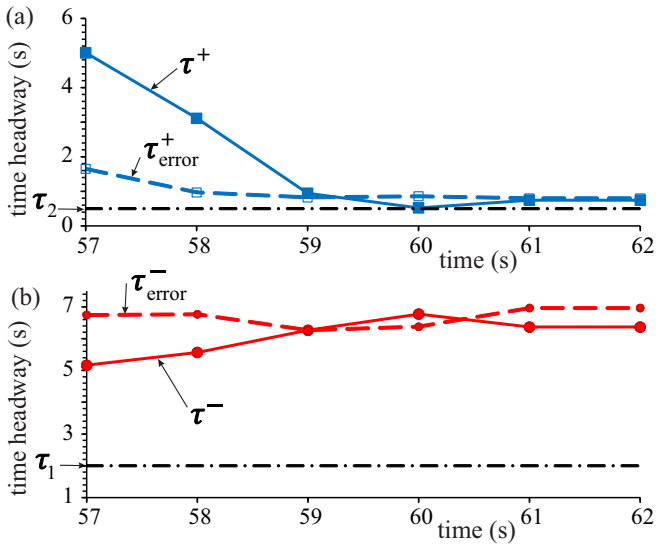

FIG. 19. Simulations of safety conditions (3) and (40) as functions of time instants t_p (22) for *first set* of realizations used in Fig. 12 ($\Delta v = 3$ m/s): (a) Time headway τ^+ (solid curve) and τ^+_{error} (dashed curve). (b) Time headway τ^- (solid curve) and τ^-_{error} (dashed curve). In (22), $t_1 = 57$ s and $p_{\text{E}} = 6$. Time headway τ^+, τ^- are given by (18) and time headway τ^+_{error}, τ^-_{error} are given by (41).

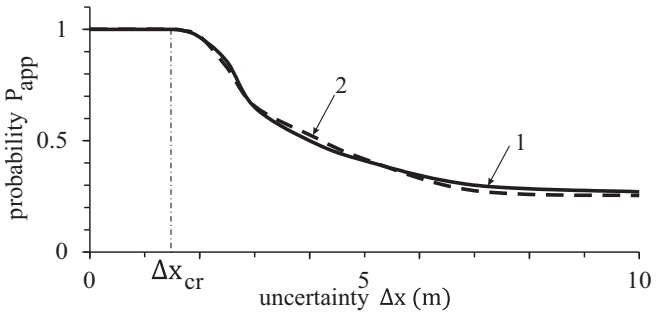

FIG. 21. Simulations of the dependence of probability P_{app} (42) on the uncertainty Δx in vehicle locations in the data of microscopic traffic situations used in Secs. IV and V. To calculate $P_{app}(\Delta x)$, $N_{app} = 200$ random sets of realizations for each of the given values of Δx have been studied (solid curve 1). The choice of $N_{app} = 200$ is explained as follows: The value of critical uncertainty $\Delta x_{cr} = 1.5$ m calculated at $N_{app} = 200$ remains at $N_{app} = 1000$ and $N_{app} = 10\,000$ (with the calculation accuracy of 0.1 m); at $\Delta x > \Delta x_{cr}$, two curves $P_{app}(\Delta x)$ calculated for $N_{app} = 200$ (solid curve 1) and $N_{app} = 1000$ (dashed curve 2) show a difference of about 5%.

B. Probability of the applicability of microscopic traffic prediction

To estimate the critical uncertainty Δx_{cr} (or Δv_{cr}), we have studied the probability of the applicability of a set of realizations for automated vehicle control with the use of the microscopic traffic prediction in a particular traffic situation. This probability denoted by P_{app} that can also be called the probability of the prediction reliability is equal to

$$P_{app} = n_{app}/N_{app}, \tag{42}$$

where N_{app} is the whole number of the sets of realizations that have been studied and n_{app} is the number of the sets of realizations in which safety conditions (3) are satisfied for each of the time instants t_p (22).

In accordance with the definition of the critical uncertainty,

$$P_{app} = 1 \quad \text{at } \Delta x \leqslant \Delta x_{cr} \ (\text{or } \Delta v \leqslant \Delta v_{cr}), \tag{43}$$

$$P_{app} < 1 \quad \text{at } \Delta x > \Delta x_{cr} \ (\text{or } \Delta v > \Delta v_{cr}). \tag{44}$$

Formula (43) determines the critical uncertainty: *Only when* the uncertainty does not exceed the critical uncertainty, i.e., $P_{app} = 1$, the microscopic traffic prediction is a reliably applicable for the automated vehicle control. Otherwise, under condition (44) with probability $1 - P_{app}$, a set of realizations can randomly occur for which the microscopic traffic prediction is not applicable for the automated vehicle control. The dependence of P_{app} on the uncertainty Δx is presented in Fig. 21. In accordance with (43), we have found that $\Delta x_{cr} = 1.5$ m. In particular, for $\Delta x = 10$ m with the probability $1 - P_{app} = 0.73$, a set of realizations can randomly occur for which the microscopic traffic prediction is not applicable for the automated vehicle control (example is shown in Fig. 15) [83].

VII. MAXIMAL CRITICAL UNCERTAINTY – PHYSICS OF OPTIMAL AUTOMATED VEHICLE MERGING

For the merging of the automated vehicle onto the priority road, the automated vehicle must decelerate to some speed $v^{(AV)}$ to ensure that the preceding vehicle (vehicle 5 in Fig. 3) had passed the intersection *and* time headway τ^+ to the preceding vehicle satisfies safety conditions (3). To increase $v^{(AV)}$, formula (31) is used that calculates the minimum time t_E at which the automated vehicle can merge onto the priority road.

The critical uncertainty and, therefore, the applicability of the microscopic traffic prediction for automated driving can be increased through another choice of the time t_E: Rather than formula (31), for the definition of time t_E we have used the approach

$$t_E = t_{E,min}(1 - \alpha_E) + t_{E,max}\alpha_E, \tag{45}$$

where α_E is a constant: $0 \leqslant \alpha_E < 1$, $t_{E,min}$ is equal to the value t_E determined through formula (31) with (23)–(25), whereas

$$t_{E,max} = \max_{n,m} (\widetilde{t}_{n,m}). \tag{46}$$

Formula (46) is also calculated under conditions (23)–(25) for the same following and preceding vehicles, which have been found through the use of formula (31). Indexes $m_{max} = m$ and $n_{max} = n - 1$, at which $\widetilde{t}_{n,m}$ in (46) reaches a maximum, allow us to find $t_{E,max}$ as

$$t_{E,max} = t_{n_{max}} + m_{max}\Delta\tau. \tag{47}$$

After $t_{E,min}$ and $t_{E,max}$ have been found, the predicted time of the merging of the automated vehicle t_E is calculated through formula (45). If no time t_E can be found, the automated vehicle decelerates with the safe speed to stop at the intersection.

The critical uncertainty Δx_{cr} can increase considerably when parameter α_E in (45) and, therefore, the predicted merging time t_E increases (Fig. 22). The physics of this result is as follows. The larger α_E is, the longer the time highway between the automated vehicle and the preceding vehicle (vehicle 5 in Fig. 13) by the automated vehicle merging onto the priority road. This causes the increase in Δx_{cr} (Fig. 22). Safety conditions (3) and, therefore, condition $P_{app} = 1$ (43) are satisfied at a larger amplitude Δx of errors in vehicle locations in the data of microscopic traffic situations as shown in Fig. 23 for $\Delta x = 12$ m that is less than $\Delta x_{cr} = 13.2$ m. This result is in contrast with the case $\alpha_E = 0$ in (45), when at a lower amplitude $\Delta x = 10$ m of errors in the data probability P_{app} is very small (value $P_{app} = 0.27$ in Fig. 21, Sec. VI B) and, therefore, the reliable application of the prediction for automated driving is not possible. However, the reliable application of the microscopic prediction with $P_{app} = 1$ (Fig. 23) is realized at the cost of the increase in the number of the time instants t_p (22) at which the microscopic prediction should be made, large random oscillations of results of the prediction (Fig. 24) as well as the decrease in the automated vehicle speed $v^{(AV)}$ (Fig. 25).

There is an optimal automated vehicle merging at which the critical uncertainty reaches its maximum value $\Delta x_{cr} = \Delta x_{cr}^{(max)} = 13.2$ m [Fig. 22(b)]; this optimal automated vehicle merging is realized at some optimal predicted merging time $t_E = t_E^{(opt)}$ reached at optimal values $\alpha_E = \alpha_E^{(opt)} = 0.4$–$0.5$

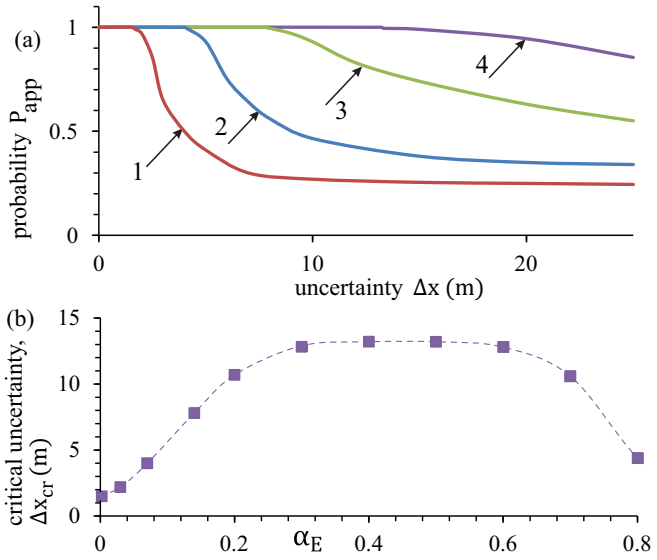

FIG. 22. Simulations of the effect of automated vehicle merging on critical uncertainty Δx_{cr}: (a) Dependencies of probability P_{app} (42) on the uncertainty Δx in vehicle locations in the data of microscopic traffic situations under the use of (45) by automated vehicle control through the microscopic traffic prediction; curve 1 for $\alpha_E = 0$ is taken from Fig. 21, curve 2: $\alpha_E = 0.07$, curve 3: $\alpha_E = 0.14$, curve 4: $\alpha_E = 0.5$. (b) Dependence of the critical uncertainty (filled squares) on value α_E in (45). To calculate $P_{app}(\Delta x)$ and Δx_{cr}, $N_{app} = 200$ random sets of realizations for each of the given values of Δx have been studied.

in (45). When t_E increases further [$t_E > t_E^{(opt)}$, i.e., in (45) $\alpha_E > \alpha_E^{(opt)}$], safety condition $\tau^- \geqslant \tau_1$ in (3) can easier fail at large errors in the data and, therefore, the critical uncertainty decreases [Fig. 22(b)].

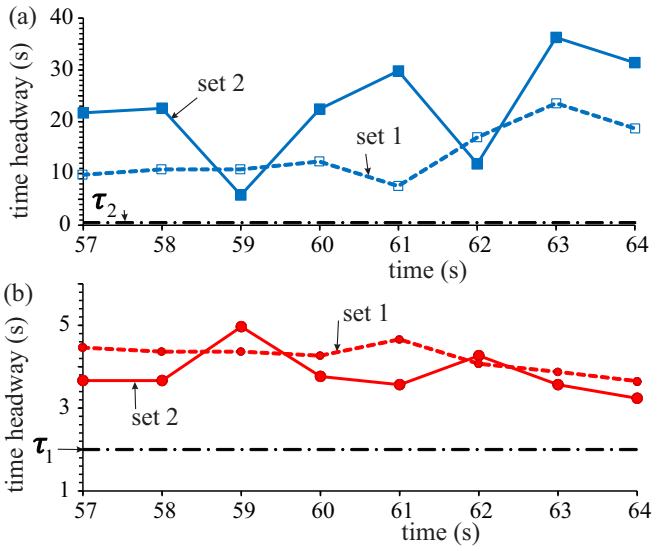

FIG. 23. Simulations of safety conditions (3) as functions of t_p (22) at $\Delta x = 12$ m and $\alpha_E = 0.5$ in (45) for two sets of realizations denoted by set 1 and set 2, respectively: Time headway τ^+ (a) and τ^- (b). In (22), $t_1 = 57$ s and $p_E = 8$.

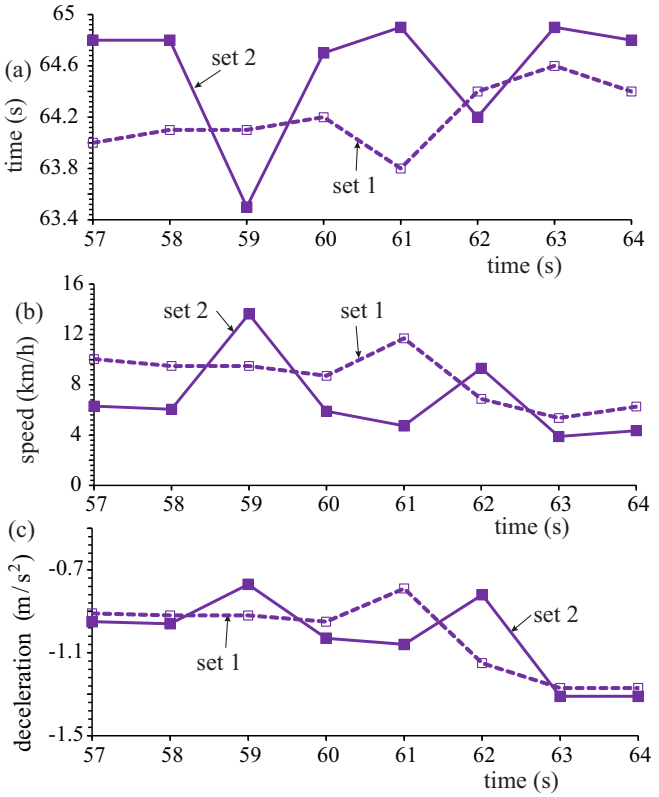

FIG. 24. Continuation of Fig. 23. Simulations of stochastic features of microscopic traffic prediction under errors in vehicle locations in the data of microscopic microscopic situations at $\Delta x = 12$ m and $\alpha_E = 0.5$ in (45). Comparison of predicted time instants of automated vehicle merging t_E (a), predicted automated vehicle speed $v^{(AV)}$ by the merging (b), and predicted automated vehicle deceleration (acceleration) (c) as functions of time instants t_p (22) for the same two sets of realizations as, respectively, those in Fig. 23: dashed curves set 1 and solid curves set 2.

Up to now, we have considered the microscopic traffic prediction with the use of only one scenario of microscopic traffic situations denoted here by *scenario 1* (dotted curves in Figs. 2(b) and 2(c)]. For a reliable analysis of statistical physics of the microscopic traffic prediction, we have studied many other scenarios. We have found that all *qualitative* physical results of the statistical physics found above for scenario 1 remain for the other scenarios. However, there are some *quantitative* differences.

An example of some important quantitative difference is shown in Figs. 26 and 27 for a scenario called *scenario 2*. For scenario 2, we have found a very small critical uncertainty $\Delta x_{cr} = 0.3$ m for $\alpha_E = 0$ in (45). To understand this result, we should note that in both scenarios 1 and 2, vehicle 5 is the preceding vehicle for the automated vehicle. Vehicle 5 should decelerate due to the merging of vehicle i [Figs. 2(b), 2(c), 26(a), and 26(b)). In scenario 1, vehicle i is the preceding vehicle for vehicle 5. Contrarily, in scenario 2 the merging of vehicle i causes the deceleration of a pair of vehicles 4 and 5 following each other. Already small errors in the locations of vehicles 4 and 5 can lead to a large error by the prediction of the location of vehicle 5 in comparison with the real location

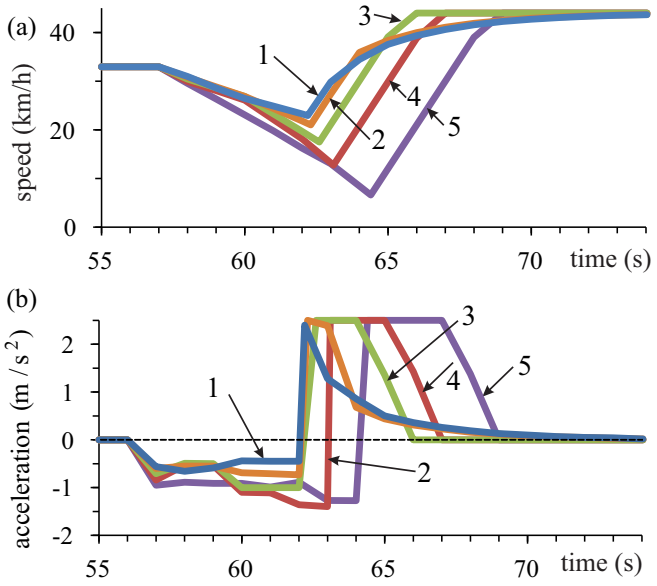

FIG. 25. Simulations of comparison of the automated vehicle speed (a) and acceleration (deceleration) (b) under the use of (45) by automated vehicle control through the microscopic traffic prediction. Curves 1 related to $\Delta x = 0$ (no data uncertainty) are taken from Fig. 6 (a) (solid curve) and (b), curves 2: $\Delta x = 1.5$ m and $\alpha_E = 0$, curves 3: $\Delta x = 4$ m and $\alpha_E = 0.07$, curves 4: $\Delta x = 7$ m and $\alpha_E = 0.14$, curves 5: $\Delta x = 12$ m for $\alpha_E = 0.5$. For all calculations, condition $\Delta x \leqslant \Delta x_{cr}$ (43) has been satisfied (Fig. 22).

of vehicle 5 in microscopic traffic situations. As a result, at $\alpha_E = 0$ in (45) conditions (3) can fail already at small errors in the data; this causes a small critical uncertainty $\Delta x_{cr} = 0.3$ m for scenario 2 (Fig. 27) in comparison with $\Delta x_{cr} = 1.5$ m for scenario 1 [Fig. 22(b)]. However, already a short increase in the merging time t_E [increase in α_E in (45)] reduces the influence of errors in the locations of vehicles 4 and 5 in scenario 2 considerably; therefore, Δx_{cr} increases sharply (Fig. 27).

We have also studied the effect on the microscopic traffic prediction caused by the existence of all three types of the uncertainty in the data discussed above (latency, errors in vehicle locations and speeds). It has been found that results derived in the paper remain qualitatively the same.

VIII. DISCUSSION

A. Some other possible applications of microscopic traffic prediction

The methodology of the microscopic traffic prediction presented and studied in this paper has been applied for a simple example of the automated vehicle that turns right at the city intersection (Fig. 1). Below we give several examples of other possible applications of the microscopic traffic prediction for automated driving [84].

(i) *The automated vehicle intends to turn left at an unsignalized intersection in an urban area.* As in Sec. III, we should make the microscopic prediction of vehicles moving on the priority road only. This prediction does not depend on the behavior of the automated vehicle.

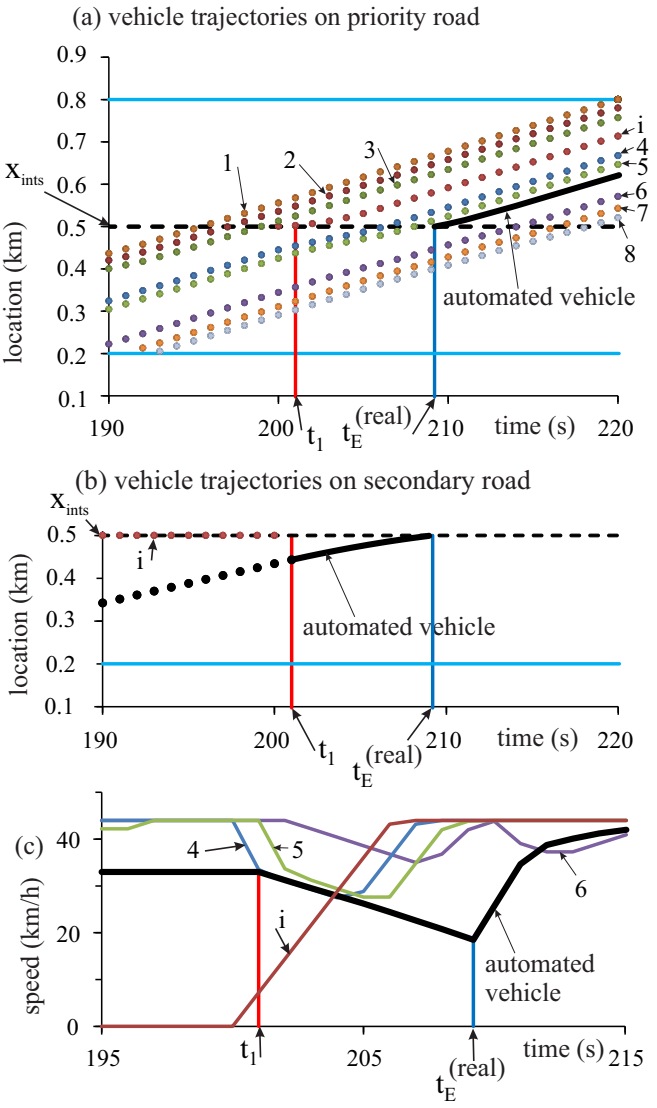

FIG. 26. Simulations of the automated vehicle control based on the microscopic traffic prediction for scenario 2 at $\alpha_E = 0$ in (45): (a), (b) Vehicle trajectories on priority road (a) and on secondary road (b); dotted curves–vehicle locations in microscopic traffic situations, solid curve–trajectory of the automated vehicle. (c) Time-dependencies of speeds of some of the vehicles. Time of the prediction beginning is $t_1 = 201$ s. Calculated values $t_E^{(real)} = 209.2$ s, $v^{(AV)}(t_E^{(real)}) = 18.5$ km/h. The flow rate on the priority and secondary roads are, respectively, 1029 and 110 vehicles/h. Time headway between preceding and following vehicles between which the automated vehicle merges in scenarios 1 (Fig. 2) and 2 are, respectively, about 6.4 s and 4.8 s. Other parameters are the same as those in Fig. 2.

(ii) *The automated vehicle intends to merge onto the main road at the on-ramp.* As in Sec. III, we should make the microscopic prediction of vehicles moving on the main road only. Thus, the predicted motion of the local neighbors on the main road does not depend on the behavior of the automated vehicle. However, even if through the earlier merging of other vehicles from the on-ramp onto the main road the motion of vehicles on the main road changes, the possible changes in

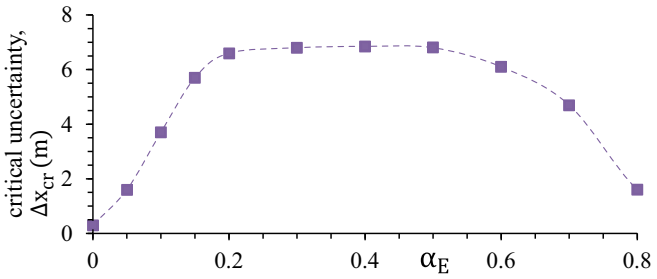

FIG. 27. Simulations of α_E function of the critical uncertainty (filled squares) calculated in accordance with formulas (42)–(45) for scenario 2 shown in Fig. 26. Maximal critical uncertainty $\Delta x_{cr} = \Delta x_{cr}^{(max)} = 6.85$ m is reached at $\alpha_E = \alpha_E^{(opt)} \approx 0.4$. In (42), $N_{app} = 200$ random sets of realizations for each of the given values of Δx have been studied. Other parameters are the same as those in Fig. 26.

the locations and speeds of the vehicles on the main road are available after the vehicle merging.

(iii) *The automated vehicle moving in the right lane that is the neighborhood one to the off-ramp lane intends to leave the main road to the off-ramp.* Although in this case the predicted motion of the local neighbors moving upstream of the automated vehicle depends on the behavior of the automated vehicle, we need the microscopic prediction of vehicles moving downstream of the automated vehicle on the main road and in the off-ramp lane only. However, the change in the motion of the automated vehicle caused by the microscopic prediction should satisfy safety conditions for the upstream vehicles (vehicles behind the automated vehicle).

(iv) *The automated vehicle moving initially in the right lane of a multi-lane road intends to pass a slow vehicle or a broken vehicle in the right lane.* As in item (iii), in this case we need the microscopic prediction of vehicles moving downstream of the automated vehicle on the main road in the right lane and the neighboring vehicles in the target lane on the main road. Thus, the moving of the upstream vehicles is not important for the accuracy of the microscopic prediction used by the automated vehicle.

It should be noted that learning algorithms as well as other methods of artificial intelligence (see, e.g., Refs. [41–58]) can be used to increase the reliability of the application of the microscopic traffic prediction. There can be here at least the following future scientific directions: (1) *the reduction of data errors* (e.g., with the use of Kalman filter) in microscopic traffic situations used as initial conditions in the microscopic traffic prediction and (2) *data fusion*, i.e., the fusion of historical data derived through the use of the methods of artificial intelligence with the data of the microscopic traffic prediction. We can assume that these applications that are out of scope of this paper can be interesting tasks for future investigations of the microscopic traffic prediction.

B. Conclusions

(1) The microscopic traffic prediction enables the control of the automated-driving vehicle in mixed traffic in a complex city traffic scenario in which the automated-driving vehicle is not able to make a decision based on a current traffic information without the use of the microscopic traffic prediction.

(2) For efficient control of the automated-driving vehicle in mixed traffic, the microscopic traffic prediction should be repeated at each of the time instants t_p (22) at which a new microscopic traffic situation is available. Therefore, the results of the microscopic traffic prediction, in particular, the predicted automated vehicle deceleration (acceleration), are used for the automated vehicle control only during a time interval $t_p \leqslant t < t_{p+1}$ (2), i.e., before the next microscopic traffic situation is available.

(3) The statistical physics of the effect of the uncertainty in the data of microscopic traffic situations on the accuracy and reliability of the microscopic traffic prediction has been revealed:

(i) The microscopic traffic prediction can guarantee collision avoidance and safety traffic even when there is a considerable data uncertainty caused by data latency, random errors of the vehicle locations, and/or random errors of the vehicle speeds in the data of microscopic traffic situations.

(ii) Due to random characteristics of the microscopic traffic prediction, there is a critical uncertainty, i.e., the maximum amplitude of errors in the data of microscopic traffic situations at which the microscopic traffic prediction can still reliably be used for the automated vehicle control.

(iii) Probability P_{app} of the reliability of the application of the microscopic traffic prediction has been found.

(iv) When the data uncertainty does not exceed the critical uncertainty, then probability $P_{app} = 1$. In this case, the microscopic traffic prediction is applicable for automated vehicle control. Contrarily, when the uncertainty exceeds the critical uncertainty, i.e., $P_{app} < 1$, however, $P_{app} > 0$, then with probability $1 - P_{app}$ there can randomly occur a realization of the microscopic traffic prediction that is not applicable for the reliable automated vehicle control.

(v) The critical uncertainty can be increased considerably through the choice of some intelligent application of the microscopic traffic prediction. However, the increase in the critical uncertainty occurs at the cost of a decrease in the automated vehicle speed.

(vi) There is some optimal automated vehicle merging at which the critical uncertainty reaches its maximum value.

(4) There can be a diverse variety of scenarios of applications of the methodology of the microscopic traffic prediction. The stochastic microscopic three-phase traffic flow model of [76,77] allows us to calculate a new microscopic prediction for the motion of the set of vehicles used in the microscopic traffic prediction for the prediction horizon 10 s during the time interval 0.005 s that is negligible short in comparison with the update time (1 s) of the data of microscopic traffic situations.

(5) The microscopic traffic prediction can lead to speed harmonization in mixed traffic flow, increase traffic safety and comfort.

ACKNOWLEDGMENTS

We thank our partners for their support in the project LUKAS—Lokales Umfeldmodell für das Kooperative, Automatisierte Fahren in komplexen Verkehrssituationen, funded by the German Federal Ministry of Economic Affairs and Climate Action.

TABLE I. Model parameters of vehicle motion used in simulations.

$\tau = 1$ s, $d = 7.5$ m/δx,
$\delta x = 0.01$ m, $\delta v = 0.01$ ms^{-1}, $\delta a = 0.01$ ms^{-2},
$v_{\text{free}}^{(\text{priority})} = 12.22$ ms$^{-1}/\delta v$ (44 km/h),
$v_{\text{free}}^{(\text{secondary})} = 9.167$ ms$^{-1}/\delta v$ (33 km/h),
$a = 0.5$ ms$^{-2}/\delta a$,
$G(u, w) = \max(0, \lfloor k\tau u + a^{-1}u(u-w)\rfloor)$,
$k = 3$, $p_1 = 0.3$, $p_b = 0.1$, $p_a = 0.17$, $p^{(0)} = 0.005$,
$p_0^{(\text{a})}(v_n) = 0.667 + 0.083 \min(1, v_n/v_{01})$,
$p_2(v_n) = 0.48 + 0.32\Theta(v_n - v_{21})$,
$v_{01} = 3$ ms$^{-1}/\delta v$, $v_{21} = 5$ ms$^{-1}/\delta v$,
$a^{(0)} = 0.2a$, $a^{(\text{a})} = a^{(\text{b})} = a$, $\Delta v_{\text{a}} = 2$ ms$^{-1}/\delta v$,
$k_{\text{a}} = 4$, $\gamma = 4$, $\Delta v_{\text{r}}^{(1)} = 2$ ms$^{-1}/\delta v$.

APPENDIX A: MODEL FOR MOTION OF HUMAN DRIVING VEHICLES IN CITY TRAFFIC

In the models (4)–(6),

$$v_{\text{c},n} = \begin{cases} v_{\text{c},n}^{(1)} & \text{at } \Delta v_n + A_{\ell,n}\tau < \Delta v_{\text{a}} \\ v_{\text{c},n}^{(2)} & \text{at } \Delta v_n + A_{\ell,n}\tau \geqslant \Delta v_{\text{a}}, \end{cases} \tag{A1}$$

$$v_{\text{c},n}^{(1)} = \begin{cases} v_n + \Delta_n^{(1)} & \text{at } g_n \leqslant G_n \\ v_n + a_n\tau & \text{at } g_n > G_n, \end{cases} \tag{A2}$$

$$\Delta_n^{(1)} = \max(-b_n\tau, \min(a_n\tau,\ \Delta v_n)), \tag{A3}$$

$$v_{\text{c},n}^{(2)} = v_n + \Delta_n^{(2)}, \tag{A4}$$

$$\Delta_n^{(2)} = k_{\text{a}} a_n \tau \max(0, \min(1,\ \gamma(g_n - v_n\tau))), \tag{A5}$$

$$a_{\max} = \begin{cases} a & \text{at } \Delta v_n + A_{\ell,n}\tau < \Delta v_{\text{a}} \\ k_{\text{a}} a & \text{at } \Delta v_n + A_{\ell,n}\tau \geqslant \Delta v_{\text{a}}, \end{cases} \tag{A6}$$

where

$$A_{n+1} = (v_{n+1} - v_n)/\tau, \quad \Delta v_n = v_{\ell,n} - v_n, \tag{A7}$$

Δv_{a}, k_{a}, and γ are constants, G_n is the synchronization space gap (see Table I); explanations of functions (A1)–(A6) have been given in Ref. [85] as well as in Sec. A.12 of Appendix A of Ref. [74]. In the model, random vehicle deceleration and acceleration are applied depending on whether the vehicle decelerates or accelerates, or else maintains its speed [76,77]:

$$\xi_n = \begin{cases} \xi_{\text{a}} & \text{if } S_{n+1} = 1 \\ -\xi_{\text{b}} & \text{if } S_{n+1} = -1 \\ \xi^{(0)} & \text{if } S_{n+1} = 0. \end{cases} \tag{A8}$$

State of vehicle motion S_{n+1} in (A8) is determined by formula

$$S_{n+1} = \begin{cases} -1 & \text{if } \tilde{v}_{n+1} < v_n \\ 1 & \text{if } \tilde{v}_{n+1} > v_n \\ 0 & \text{if } \tilde{v}_{n+1} = v_n. \end{cases} \tag{A9}$$

In (A8), ξ_{b}, $\xi^{(0)}$, and ξ_{a} are random sources for deceleration and acceleration that are as follows [76,77]:

$$\xi_{\text{b}} = a^{(\text{b})}\tau\Theta(p_{\text{b}} - r), \tag{A10}$$

$$\xi^{(0)} = a^{(0)}\tau \begin{cases} -1 & \text{if } r < p^{(0)} \\ 1 & \text{if } p^{(0)} \leqslant r < 2p^{(0)} \\ 0 & \text{otherwise} \end{cases} \quad \text{and } v_n > 0 \tag{A11}$$

$$\xi_{\text{a}} = a^{(\text{a})}\tau\Theta(p_{\text{a}} - r), \tag{A12}$$

p_{b} is probability of random vehicle deceleration, p_{a} is probability of random vehicle acceleration, $p^{(0)}$ and $a^{(0)} \leqslant a$ are constants, $r = \text{rand}(0, 1)$, $\Theta(z) = 0$ at $z < 0$ and $\Theta(z) = 1$ at $z \geqslant 0$, $a^{(\text{a})}$ and $a^{(\text{b})}$ are model parameters (Table I).

To simulate time delays either in vehicle acceleration or in vehicle deceleration, a_n and b_n are the following stochastic functions [76,77]:

$$a_n = a\Theta(P_0 - r_1), \tag{A13}$$

$$b_n = a\Theta(P_1 - r_1), \tag{A14}$$

$$P_0 = \begin{cases} p_0 & \text{if } S_n \neq 1 \\ 1 & \text{if } S_n = 1, \end{cases} \tag{A15}$$

$$P_1 = \begin{cases} p_1 & \text{if } S_n \neq -1 \\ p_2 & \text{if } S_n = -1, \end{cases} \tag{A16}$$

$r_1 = \text{rand}(0, 1)$, p_1 is constant, $p_2 = p_2(v_n)$ is a speed function (see Table I). Equation (A13) with $P_0 = p_0 < 1$ is applied only if the vehicle did not accelerate at the former time step ($S_n \neq 1$); in the latter case, a vehicle accelerates only with some probability p_0 (A15).

To calculate probability P_{app} (42) of the applicability of a set of realizations for the automated vehicle control with the use of the microscopic traffic prediction (Fig. 22), we should exclude simulation realizations in which rather than random errors in the data of microscopic traffic situations, model fluctuations determine probability P_{app}. Such a case can theoretically occur when due to probability of delay in acceleration $1 - p_0$ there appears randomly a successive number of time steps denoted by κ, when a vehicle does not accelerate. Therefore, for the microscopic traffic prediction the value of κ should be limited in the model. To reach this goal, we introduce in our model a new variable κ_n [86]:

$$\kappa_{n+1} = \begin{cases} \kappa_n + 1 & \text{if } S_n \neq 1 \text{ and } v_{\text{s},n} > v_n \\ & \text{and } (v_{\ell,n} > v_n \text{ or } g_n > G_n) \\ 0 & \text{otherwise.} \end{cases} \tag{A17}$$

Then, probability p_0 in (A15) is formulated as follows:

$$p_0 = \begin{cases} p_0^{(\text{a})}(v_n) & \text{if } \kappa_{n+1} < 2 \\ 1 & \text{if } \kappa_{n+1} \geqslant 2. \end{cases} \tag{A18}$$

Thus, due to formulas (A17) and (A18), the successive number of time steps of the delay in acceleration of a vehicle is limited by $\kappa = 1$. As proven in simulations, this change in the model fluctuation description ensures that in the absence of errors in the data (i.e., $\Delta x = \Delta v = 0$) the probability P_{app} (42) is equal to 1. Therefore, only due to the appearance of large enough errors in the data formula (44) can be valid. The mean time delay in vehicle acceleration is equal to

$$\tau_{\text{del}}^{(\text{acc})}(v_n) = \left(2 - p_0^{(\text{a})}(v_n)\right)\tau. \tag{A19}$$

From formula (A19), it follows that the mean time delay in vehicle acceleration from a standstill within a wide moving jam, when in formula (A19) the speed $v_n = 0$ (in traffic flow modeling, the time delay in acceleration is related to a

slow-to-start rule [88,89]), is equal to

$$\tau_{\rm del}^{\rm (acc)}(0) = \big(2 - p_0^{\rm (a)}(0)\big)\tau. \tag{A20}$$

As in Refs. [76,77], probability $p_0^{\rm (a)}(v_n)$ in (A18) is chosen to be an increasing speed function (Table I). Because the speed within synchronized flow is larger than zero, the mean time delay in vehicle acceleration at the downstream front of synchronized flow that we denote by

$$\tau_{\rm del,\ syn}^{\rm (acc)} = \tau_{\rm del}^{\rm (acc)}(v_n), \quad v_n > 0 \tag{A21}$$

is shorter than the mean time delay in vehicle acceleration at the downstream front of the wide moving jam $\tau_{\rm del}^{\rm (acc)}(0)$:

$$\tau_{\rm del,\ syn}^{\rm (acc)} < \tau_{\rm del}^{\rm (acc)}(0). \tag{A22}$$

As in Refs. [76,77], the safe speed $v_{{\rm s},n}$ in (4) is chosen in the form

$$v_{{\rm s},n} = \min\big(v_n^{\rm (safe)}, g_n/\tau + v_\ell^{\rm (a)}\big), \tag{A23}$$

where $v_\ell^{\rm (a)}$ is an anticipation speed of the preceding vehicle, the function

$$v_n^{\rm (safe)} = \lfloor v^{\rm (safe)}(g_n,\ v_{\ell,n})\rfloor, \tag{A24}$$

$v^{\rm (safe)}(g_n,\ v_{\ell,n})$ in (A24) is related to a safe speed in models by Gipps [90] and Krauß *et al.* [91,92]; a detailed consideration of the functions $v^{\rm (safe)}(g_n,\ v_{\ell,n})$ and $v_\ell^{\rm (a)}$ has been presented in Sec. A.3.5 of Appendix A of the book [74]. When a vehicle moving in the secondary road is the closest one to the intersection, $v_{{\rm s},n}$ is chosen as

$$v_{{\rm s},n} = \big\lfloor v^{\rm (safe)}(x_{\rm ints} - x_n, 0)\big\rfloor. \tag{A25}$$

APPENDIX B: MODEL FOR VEHICLE MERGING AT ROAD INTERSECTION

1. Merging of human driving vehicles

The following rules for merging human-driving vehicles from the secondary road onto the priority road at the intersection are used:

$$g_n^+ > \min\left(\hat v_n\tau,\ G(\hat v_n, v_n^+)\right), \tag{B1}$$

$$g_n^- > \min\left(v_n^-\tau, G(v_n^-, \hat v_n)\right), \tag{B2}$$

$$x_{n-1} = x_{\rm ints},\quad v_{n-1} = 0. \tag{B3}$$

In (B1)–(B3),

$$g_n^+ = x_n^+ - x_{\rm ints} - d, \tag{B4}$$

$$g_n^- = x_{\rm ints} - x_n^- - d, \tag{B5}$$

$$\hat v_n = \min\big(v_n^+, v_n + \Delta v_r^{(1)}\big), \tag{B6}$$

$\Delta v_r^{(1)}$ is a constant (Table I).

2. Merging of automated vehicle onto priority road without the use of prediction

Rules for merging the automated vehicle from the secondary road onto the priority road are as follows:

$$\widetilde g_{n,m}^+ \geqslant \hat v_n\tau_2, \tag{B7}$$

where $\hat v_n$ is given by (B6) in which v_n should be replaced by $v_n^{\rm (AV)}$,

$$\widetilde g_{n,m}^- \geqslant v_n^-\tau_1, \tag{B8}$$

$$x_{n-1} = x_{\rm ints},\quad v_{n-1} = 0. \tag{B9}$$

Conditions (B7) and (B8) correspond to (3). In (B7)–(B9),

$$\widetilde g_{n,m}^+ = \widetilde x_{n,m}^+ - x_{\rm ints} - d, \tag{B10}$$

$$\widetilde g_{n,m}^- = x_{\rm ints} - \widetilde x_{n,m}^- - d, \tag{B11}$$

$$\widetilde x_{n,m}^+ = x_{n-1}^+ + v_n^+ m\Delta\tau,\quad m = 1, 2, \ldots, M, \tag{B12}$$

$$\widetilde x_{n,m}^- = x_{n-1}^- + v_n^- m\Delta\tau,\quad m = 1, 2, \ldots, M. \tag{B13}$$

Conditions (B7)–(B9) with (B10)–(B13) are checked for all indexes $m = 1, 2, \ldots, M$. If for one of the values m these conditions are satisfied, the automated vehicle merges onto the priority road with the speed $v_n^{\rm (AV)} = \hat v_n$, where $\hat v_n$ is given by (B6) with $\Delta v_{\rm r}^{(1)} = a_{\rm max}^{\rm (AV)}\tau(1 - m/M)$. For each of the M short time steps $\Delta\tau$, the location of a vehicle that is the preceding vehicle for the automated vehicle is given by a linear approximation (B12) between points x_n^+ and x_{n-1}^+; the similar formula (B13) is used for the following vehicle.

APPENDIX C: SOME CHARACTERISTICS OF AUTOMATED DRIVING

1. Prediction of time instants $t_{\rm min}, t_{\rm max}$ and automated vehicle deceleration

To predict $t_{\rm min}$ and $t_{\rm max}$ at each of the time instants t_p (22), the automated vehicle motion is predicted between the current location of the automated vehicle $x^{\rm (AV)}(t_{\rm p})$ and intersection location $x_{\rm ints}$. The rules (8)–(11) are used for the prediction. To find $t_{\rm min}$, the automated vehicle motion is simulated, when the safe speed in (10) at $\widetilde t_n \geqslant t_{\rm p}$ is chosen to be equal to the maximum speed, $v_{{\rm s},n} = v_{\rm free}^{\rm (secondary)}$, and acceleration $a_{\rm n}^{\rm (AV)}$ in (9) is equal to

$$a_n^{\rm (AV)} = a_{\rm max}^{\rm (AV)}. \tag{C1}$$

To find $t_{\rm max}$, the acceleration $a_n^{\rm (AV)}$ in (9) is given by (C1) and the safe speed in (10) is given by (A25). The prediction horizon is equal to

$$\Delta T_{\rm p} = t_{\rm max} - t_{\rm p},\ p = 1, 2, \ldots, p_{\rm E}. \tag{C2}$$

If time $t_{\rm E}$ is found from Eq. (45), the value $t_{\rm E}$ is used to calculate predicted deceleration $b_{\rm p}$ required for the automated vehicle to reach location $x_{\rm ints}$ at time $t_{\rm E}$,

$$b_{\rm p} = \left\lfloor \frac{2(x_{\rm ints} - x^{\rm (AV)}(t_{\rm p}) - v^{\rm (AV)}(t_{\rm p})(T + \delta T))}{T(T+\tau) + 2(T + \delta T)\delta T} \right\rfloor, \tag{C3}$$

where

$$p = 1, 2, \ldots, p_{\rm E} - 1, \tag{C4}$$

T and δT are, respectively, the integer and the fractional parts of time $T_{\rm E} = t_{\rm E}(t_p) - t_p$: $T = \tau\lfloor T_{\rm E}/\tau\rfloor$, $\delta T = T_{\rm E} - T$.

The microscopic traffic prediction is made until the following inequality:

$$t_{\mathrm{E}}(t_{\mathrm{p_E}}) - t_{\mathrm{p_E}} < \tau \tag{C5}$$

has satisfied. Index $p = p_{\mathrm{E}}$ found from (C5) corresponds to the maximum time instant $t_{\mathrm{p}} = t_{\mathrm{p_E}}$ at which the last microscopic traffic prediction is performed.

2. Merging of automated vehicle onto priority road based on prediction

After condition (C5) has been satisfied, the automated vehicle moves with deceleration $b_{\mathrm{p}} = b_{\mathrm{p_E}-1}$ (C3) in accordance with rules (20), (21), and (11) until the automated vehicle merges onto the priority road. The time instant $t_{\mathrm{E}}^{(\mathrm{real})}$ at which the automated vehicle merges onto the priority road is found from conditions (B7), (B8), and (B10)–(B13) together with condition

$$x^{(\mathrm{AV})}(t_{\mathrm{p_E}}) + v^{(\mathrm{AV})}(t_{\mathrm{E}}^{(\mathrm{real})})m\Delta\tau \geqslant x_{\mathrm{ints}}, \tag{C6}$$

where $m = 0, 1, 2, \ldots, M$, the speed $v^{(\mathrm{AV})} = v^{(\mathrm{AV})}(t_{\mathrm{E}}^{(\mathrm{real})})$ is found as

$$v^{(\mathrm{AV})}\left(t_{\mathrm{E}}^{(\mathrm{real})}\right) = \max\left(0, \min\left(v_{\mathrm{free}}, v^{(\mathrm{AV})}(t_{p_{\mathrm{E}}}) - b_{p_{\mathrm{E}}-1}m\Delta\tau\right)\right). \tag{C7}$$

Conditions (B7), (B8), and (B10)–(B13) together with (C6) and (C7) are checked for different steps $m = 0, 1, 2, \ldots, M$ to find a minimum value $m = m_{\mathrm{E}}^{(\mathrm{real})}$ for which conditions (B7), (B8), (B10)–(B13), (C6), and (C7) are satisfied. Then, the time instant $t_{\mathrm{E}}^{(\mathrm{real})}$ at which the automated vehicle merges onto the priority road is equal to [93]

$$t_{\mathrm{E}}^{(\mathrm{real})} = t_{p_{\mathrm{E}}} + m_{\mathrm{E}}^{(\mathrm{real})}\Delta\tau. \tag{C8}$$

After the automated vehicle has turned right onto the priority road, it moves in accordance with (8)–(10). It should be emphasized that in condition (B7) used for the calculation of formulas (C6)–(C8) instead of formula (B6) the following formula has been used $\hat{v}_n = v^{(\mathrm{AV})}$.

[1] A. Reuschel, Österr. Ing.-Arch. **4**, 193 (1950).
[2] A. Reuschel, Z. Österr, Ing.-Archit.-Ver. **95**, 59 (1950).
[3] A. Reuschel, Z. Österr, Ing.-Archit.-Ver. **95**, 73 (1950).
[4] L. A. Pipes, J. Appl. Phys. **24**, 274 (1953).
[5] E. Kometani and T. Sasaki, J. Oper. Res. Soc. Jap. **2**, 11 (1958).
[6] E. Kometani and T. Sasaki, Oper. Res. **7**, 704 (1959).
[7] E. Kometani and T. Sasaki, Oper. Res. Soc. Jap. **3**, 176 (1961).
[8] E. Kometani and T. Sasaki, in *Theory of Traffic Flow*, edited by R. Herman (Elsevier, Amsterdam, 1961), pp. 105–119
[9] R. E. Chandler, R. Herman, and E. W. Montroll, Oper. Res. **6**, 165 (1958).
[10] R. Herman, E. W. Montroll, R. B. Potts, and R. W. Rothery, Oper. Res. **7**, 86 (1959).
[11] D. C. Gazis, R. Herman, and R. B. Potts, Oper. Res. **7**, 499 (1959).
[12] D. C. Gazis, R. Herman, and R. W. Rothery, Oper. Res. **9**, 545 (1961).
[13] G. F. Newell, Oper. Res. **9**, 209 (1961).
[14] D. Chowdhury, L. Santen, and A. Schadschneider, Phys. Rep. **329**, 199 (2000).
[15] D. Helbing, Rev. Mod. Phys. **73**, 1067 (2001).
[16] T. Nagatani, Rep. Prog. Phys. **65**, 1331 (2002).
[17] K. Nagel, P. Wagner, and R. Woesler, Oper. Res. **51**, 681 (2003).
[18] W. D. Ashton, *The Theory of Traffic Flow* (Methuen & Co. London, John Wiley & Sons, New York, 1966).
[19] D. L. Gerlough and M. J. Huber, *Traffic Flow Theory Special Report 165* (Transp. Res. Board, Washington, D.C., 1975).
[20] D. C. Gazis, *Traffic Theory* (Springer, Berlin, 2002).
[21] A. Schadschneider, D. Chowdhury, and K. Nishinari, *Stochastic Transport in Complex Systems* (Elsevier Science Inc., New York, 2011).
[22] M. Treiber and A. Kesting, *Traffic Flow Dynamics* (Springer, Berlin, 2013)
[23] J. Barceló (ed.), *Fundamentals of Traffic Simulation* (Springer, Berlin, 2010).
[24] L. Elefteriadou, *An Introduction to Traffic Flow Theory* (Springer, Berlin, 2014).
[25] Daiheng Ni, *Traffic Flow Theory: Characteristics, Experimental Methods, and Numerical Techniques* (Elsevier, Amsterdam, 2015); F. Kessels, *Traffic Flow Modelling* (Springer, Berlin, 2019).
[26] *Automated Highway Systems*, edited by P. A. Ioannou (Plenum Press, New York, 1997).
[27] P. A. Ioannou and J. Sun, *Robust Adaptive Control* (Prentice Hall, Inc., Upper Saddle River, New Jersey, 1996).
[28] P. A. Ioannou and C. C. Chien, IEEE Trans. Veh. Technol. **42**, 657 (1993).
[29] G. Meyer and S. Beiker, *Road Vehicle Automation* (Berlin, Springer, 2014).
[30] C.-Y. Liang and H. Peng, JSME Jnt. J. Ser. C **43**, 671 (2000).
[31] L. C. Davis, Physica A **405**, 128 (2014).
[32] E. Yurtsever, J. Lambert, A. Carballo, and K. Takeda, IEEE Access **8**, 58443 (2020).
[33] D. González, J. Pérez, V. Milanés, and F. Nashashibi, IEEE Trans. Intell. Transp. Syst. **17**, 1135 (2016).
[34] X. Zhao, J. Wang, G. Yin, K. Zhang, in *2019 IEEE Intelligent Transportation Systems Conference (ITSC)* (IEEE, Auckland, New Zealand, 2019), pp. 2121–2126.
[35] M. R. Hafner, D. Cunningham, L. Caminiti, and D. Del Vecchio, IEEE Trans. Intell. Transp. Syst. **14**, 1162 (2013).
[36] R. Schmitz, M. Torrent-Moreno, H. Hartenstein, and W. Effelsberg, in *29th Annual IEEE International Conference on Local Computer Networks* (IEEE, Tampa, Florida, USA, 2004), pp. 594–601.
[37] J. Maurer, T. Fuegen, and W. Wiesbeck, in *11th European Wireless Conference 2005–Next Generation Wireless and Mobile Communications and Services* (VDE-Verlag, Berlin, Germany, 2006), pp. 1–7.
[38] Q. Chen, D. Jiang, V. Taliwal, and L. Delgrossi, in *Proceedings of the 3rd International Workshop on Vehicular ad hoc Networks (VANET '06)*, (Association for Computing Machinery, New York, 2006), pp. 50–56.

[39] T.-H. Wang, S. Manivasagam, M. Liang, B. Yang, W. Zeng, and R. Urtasun, in *Computer Vision–ECCV 2020. ECCV 2020*, Lecture Notes in Computer Science, Vol. 12347 edited by A. Vedaldi, H. Bischof, T. Brox, JM. Frahm. (Springer, Cham, 2020).

[40] *Vehicular Communications and Networks*, edited by W. Chen (Woodhead Publishing, Cambridge, 2015).

[41] S. Brechtel, T. Gindele, R. Dillmann, in *17th IEEE International Conference on Intelligent Transportation Systems, ITSC 2014* (IEEE, Qingdao, China, 2014), pp. 392–399.

[42] X. Lin, J. Zhang, J. Shang, Y. Wang, H. Yu, X. Zhang, in *2019 IEEE Intelligent Transportation Systems Conference, ITSC 2019* (IEEE, Auckland, New Zealand, 2019), pp. 2449–2455.

[43] P. Schorner, L. Tottel, J. Doll, and J. M. Zollner, in *Proceedings of IEEE Intelligent Vehicles Symposium* (IEEE, Paris, France, 2019), pp. 2299–2306.

[44] D. Klimenko, J. Song, and H. Kurniawati, in *Australasian Conference on Robotics and Automation, ACRA* (The University of Melbourne, Melbourne, Australia, 2014), Vol. 02-04-Dece.

[45] P. Schorner, L. Tottel, J. Doll, and J. M. Zollner, in *Proceedings of IEEE Intel. Veh. Symposium* (IEEE, Paris, France, 2019), pp. 2172–2179.

[46] D. Isele, R. Rahimi, A. Cosgun, K. Subramanian, and K. Fujimura, in *Proceedings - IEEE International Conference on Robotics and Automation* (IEEE, Brisbane, Australia, 2018), pp. 2034–2039.

[47] Z. Qiao, K. Muelling, J. Dolan, P. Palanisamy, P. Mudalige, in *Proceedings of IEEE Conference on Intelligent Transportation Systems, ITSC* (IEEE, Maui, Hawaii, USA, 2018), Vol. 2018-Novem, pp. 2377–2382.

[48] K. Sama, Y. Morales, H. Liu, N. Akai, A. Carballo, E. Takeuchi, K. Takeda, IEEE Transactions on Vehicular Technology **69**, 9315 (2020).

[49] P. F. Orzechowski, A. Meyer, M. Lauer, in *IEEE Conference on Intelligent Transportation Systems, ITSC* (IEEE, Maui, Hawaii, USA, 2018), pp. 1729–1736.

[50] M. Althoff and S. Magdici, IEEE Trans. Intell. Veh. **1**, 187 (2016).

[51] M. Naumann, H. Konigshof, M. Lauer, and C. Stiller, in *Proceedings of IEEE Intelligent Vehicles Symposium* (IEEE, Paris, France, 2019), pp. 140–145.

[52] Ö. S. Tas and C. Stiller, in *Proceedings of IEEE Intelligent Vehicles Symposium* (IEEE, Changshu, China, 2018), pp. 1171–1178.

[53] Y. Akagi and P. Raksincharoensak, in *Proceedings of IEEE Intelligent Vehicles Symposium* (IEEE, Seoul, Korea, 2015), pp. 368–373.

[54] Y. Morales, Y. Yoshihara, N. Akai, E. Takeuchi, and Y. Ninomiya, in *Proceedings of IEEE Intelligent Vehicles Symposium* (IEEE, Los Angeles, CA, USA, 2017), pp. 901–907.

[55] Y. Morales, Y. Yoshihara, N. Akai, E. Takeuchi, and Y. Ninomiya, in *IEEE International Conference on Intelligent Robots and Systems* (IEEE, Vancouver, BC, Canada, 2017), pp. 3452–3459.

[56] E. Takeuchi, Y. Yoshihara, and N. Yoshiki, in *Proceedings of IEEE Conference on Intelligent Transportation Systems, ITSC* (IEEE, Las Palmas, Spain, 2015), pp. 2311–2316.

[57] M. Y. Yu, R. Vasudevan, and M. Johnson-Roberson, IEEE Rob. Autom. Lett. **4**, 2235 (2019).

[58] S. Hoermann, F. Kunz, D. Nuss, S. Renter, K. Dietmayer, in *Proceedings of IEEE Intelligent Vehicles Symposium* (IEEE, Los Angeles, CA, USA, 2017), pp. 727–732.

[59] The methodology of microscopic traffic prediction has been discussed at IEEE Conferences: B. S. Kerner, S. L. Klenov, in *2021 Systems of Signals Generating and Processing in the Field of on Board Communications*, pp. 1–4, 2021; *2022 Systems of Signals Generating and Processing in the Field of on Board Communications* (IEEE, Moscow, Russia, 2022), pp. 1–6.

[60] The time-discrete traffic flow model for mixed traffic (Sec. II C) calculates a new microscopic traffic prediction for the motion of about 30 vehicles during a time interval $\theta < 0.005$ s, which is negligibly short in comparison with time interval $\delta t = t_{p+1} - t_p = \tau = 1$ s and the prediction horizon $\Delta T_p = 10$ s used in simulations.

[61] S. Dharba and K. R. Rajagopal, Transp. Res. C **7**, 329 (1999).

[62] A. Bose and P. Ioannou, Transp. Res. C **11**, 439 (2003).

[63] A. Kesting, M. Treiber, M. Schönhof, and D. Helbing, Transp. Res. Rec. **2000**, 16 (2007).

[64] A. Kesting, M. Treiber, M. Schönhof, and D. Helbing, Transp. Res. C **16**, 668 (2008).

[65] A. Kesting, M. Treiber, and D. Helbing, Phil. Trans. R. Soc. A. **368**, 4585 (2010).

[66] S. Kukuchi, N. Uno, and M. Tanaka, J. Transp. Eng. **129**, 146 (2003).

[67] P. Y. Li and A. Shrivastava, Transp. Res. C **10**, 275 (2002).

[68] G. Marsden, M. McDonald, and M. Brackstone, Transp. Res. C **9**, 33 (2001).

[69] J.-J. Martinez and C. Canudas-do-Wit, IEEE Trans. Control. Syst. Technol. **15**, 246 (2007).

[70] S. E. Shladover, Veh. Syst. Dyn. **24**, 551 (1995).

[71] S. E. Shladover, D. Su, and X.-T. Lu, Transp. Res. Rec. **2324**, 63 (2012).

[72] A. Talebpour and H. S. Mahmassani, Transp. Res. C **71**, 143 (2016).

[73] B. S. Kerner, Phys. Rev. E **97**, 042303 (2018); Physica A **562**, 125315 (2021).

[74] B. S. Kerner, *Breakdown in Traffic Networks* (Springer, Berlin, New York, 2017).

[75] B. S. Kerner, *Understanding Real Traffic: Paradigm Shift in Transportation Science* (Springer, Cham, Switzerland 2021).

[76] B. S. Kerner and S. L. Klenov, J. Phys. A: Math. Gen. **35**, L31 (2002); Phys. Rev. E **68**, 036130 (2003).

[77] B. S. Kerner and S. L. Klenov, Phys. Rev. E **80**, 056101 (2009).

[78] Vehicle coordinates, speeds, and acceleration (deceleration) are measured, respectively, in units of δx, δv, and δa, where $\delta x =$ 0.01 m, $\delta v = \delta x/\tau$, $\delta a = \delta v/\tau$.

[79] W. Helly, in *Proceedings of the Symposium on Theory of Traffic Flow*, (Research Laboratories, General Motors, Elsevier, Amsterdam, 1959), pp. 207–238.

[80] Rather than all vehicle data measured in the red dashed road region shown in Fig. 1(a), to decrease the communication costs in possible *engineering applications* of the microscopic traffic prediction, a smaller data set from vehicles moving around the automated vehicle might be sufficient to be defined. In the paper, to find physical features of the microscopic traffic prediction, we have neglected this point while considering all measured vehicle data. However, from simulation results, we can conclude that the motion of about ten vehicles is only needed for the microscopic traffic prediction. A precise def-

inition of the set of vehicles used in the microscopic traffic prediction can be an interesting task for future investigations.

[81] In simulations, in addition to this condition, to determine the beginning of the microscopic traffic prediction $t_{\rm p} = t_1$, we have used the condition that the distance from the current automated vehicle location $x^{(\rm AV)}(t_{\rm p})$ to the location $x_{\rm ints}$ of the road intersection is less than some given value L_1 (where $L_1 = 0.15$ km), i.e., $x_{\rm ints} - x^{(\rm AV)}(t_{\rm p}) < L_1$ that is satisfied in all simulation results presented.

[82] If the microscopic traffic prediction would be applied for the automated traffic control in *real engineering applications* under uncertainty in the data, we cannot know whether safety conditions (3) are satisfied or not. Contrary to real engineering applications, in *the theory* of the microscopic traffic prediction, we prove safety conditions (3) at each of the time instants t_p (22). The cause of this proof is as follows. It allows us to distinguish between two cases: (i) a *reliable application* of the microscopic traffic prediction, when additionally to the satisfaction of safety conditions (40), safety conditions (3) are also satisfied at each of the time instants t_p (22) and (ii) an application of the microscopic traffic prediction that cannot be considered as a reliable one, when safety conditions (3) are not satisfied at least for one of the time instants t_p (22) at which the prediction is calculated.

[83] A dependence of $P_{\rm app}$ on the uncertainty Δv studied (not shown in the paper) leads to the conclusion that $\Delta v_{\rm cr} = 0.7$ m/s. For $\Delta v = 3$ m/s, the probability of the occurrence of the set of realizations for which the microscopic traffic prediction cannot be used for a reliable automated vehicle control is $1 - P_{\rm app} = 0.56$ (example is shown in Fig. 20).

[84] In the paper, we have used microscopic traffic prediction for the automated vehicle control. Generally, the same methodology of the microscopic traffic prediction can be used for the motion of a human-driving vehicle that can be considered a subject vehicle. The subject vehicle performs the microscopic traffic prediction of the motion of other vehicles around it. Contrary to the automated vehicle control, a driver of the subject vehicle decides by themselves whether and how she/he uses the microscopic traffic prediction for a safety driving.

[85] B. S. Kerner, Europhys. Lett. **102**, 28010 (2013); Physica A **397**, 76 (2014).

[86] To our knowledge, a model variable—a successive number of time steps within which a stopped vehicle delays its acceleration was introduced by Jiang and Wu in a cellular automation traffic flow model [87].

[87] R. Jiang and Q. S. Wu, J. Phys. A: Math. Gen. **36**, 381 (2003).

[88] R. Barlović, L. Santen, A. Schadschneider, and M. Schreckenberg, Eur. Phys. J. B **5**, 793 (1998).

[89] M. Takayasu and H. Takayasu, Fractals **01**, 860 (1993).

[90] P. G. Gipps, Trans. Res. B **15**, 105 (1981).

[91] S. Krauß, DRL-Forschungsbericht 98-08, Ph.D. thesis, 1998, https://sumo.dlr.de/pdf/KraussDiss.pdf, Deutsches Zentrum für Luft–und Raumfahrt (DLR), Berlin.

[92] S. Krauß, P. Wagner, and C. Gawron, Phys. Rev. E **55**, 5597 (1997).

[93] If the speed $v^{(\rm AV)}$ at the time instant $t_{\rm E}^{(\rm real)}$ (C8) at which the automated vehicle really merges onto the priority road is larger than the speed of the preceding vehicle v^+, the speed of the automated vehicle is sets to $v^{(\rm AV)} = v^+$; however, such a possible case has not been found in simulations presented in the paper.